

**ANTI WETTING AND ANTIFOULING JANUS MEMBRANE
FOR DESALINATION OF SALINE OILY WASTEWATER
BY MEMBRANE DISTILLATION**

by

Chenxi Li

B.E.Sc., The University of Western Ontario, 2017

B.E., Zhejiang University of Technology, 2017

A THESIS SUBMITTED IN PARTIAL FULFILLMENT OF
THE REQUIREMENTS FOR THE DEGREE OF

MASTER OF APPLIED SCIENCE

in

THE FACULTY OF GRADUATE AND POSTDOCTORAL STUDIES
(Civil Engineering)

THE UNIVERSITY OF BRITISH COLUMBIA
(Vancouver)

August 2019

© Chenxi Li, 2019

The following individuals certify that they have read, and recommend to the Faculty of Graduate and Postdoctoral Studies for acceptance, a thesis/dissertation entitled:

Antiwetting and Antifouling Janus Membrane for Desalination of Saline Oily Wastewater by
Membrane Distillation

submitted by Chenxi Li in partial fulfillment of the requirements for
the degree of Master of Applied Science
in Civil Engineering

Examining Committee:

Jongho Lee, Civil Engineering

Supervisor

Supervisory Committee Member

Supervisory Committee Member

Ryan Ziels, Civil Engineering

Additional Examiner

Additional Supervisory Committee Members:

Supervisory Committee Member

Supervisory Committee Member

Abstract

Membrane distillation (MD) is an emerging desalination technology employing a hydrophobic (water-repelling) microporous membrane that is promising for water reclamation from highly saline streams that conventional reverse osmosis (RO) cannot treat. However, conventional hydrophobic membranes are prone to wetting and fouling when treating complex waste streams, such as oil- and gas-produced waters, which limits the applications of MD.

Typically, two conflicting surface properties (i.e., hydrophobic and hydrophilic) are required to mitigate pore wetting and membrane fouling, respectively. In this thesis, we develop Janus membranes comprising a hydrophilic zwitterionic polymer layer and an omniphobic (all liquid-repelling) porous substrate that simultaneously possess fouling and wetting resistances. An omniphobic membrane was first fabricated by attaching silica nanoparticles (SiNPs) to the fibers of a quartz fiber mat, creating multilevel re-entrant structures, followed by surface fluorination to reduce the surface energy. The Janus membrane was then fabricated by grafting a zwitterionic polymer brush layer via surface-initiated atom-transfer radical-polymerization (ATRP) on the omniphobic substrate.

Membrane characterizations, including Fourier-transform infrared spectroscopy, fluorescence microscopy, and contact angle measurements, confirm that the surface hydrophilicity can be finely tuned by adjusting the duration of the ATRP reaction. Also, the zwitterionic polymer brush layer was confined on the top surface of the Janus membrane, rendering the surface hydrophilic, while the remaining part of the Janus membrane remained omniphobic, resisting the wicking of low-surface-tension liquids including ethanol and hexane. A static oil-fouling test showed that crude oil droplets irreversibly fouled an omniphobic membrane (without a hydrophilic top layer) in water. In contrast, oil droplets placed on the Janus membrane in air were immediately desorbed upon its immersion in water. Finally, we performed direct-contact MD (DCMD) experiments using a crude-oil-in-saline (NaCl) water emulsion as a feed solution, simulating highly saline oily wastewater. The Janus membrane exhibited superior wetting and fouling resistances, with stable water flux and nearly perfect salt rejection, while an omniphobic membrane failed in the desalination process. Our work highlights the great potential of antiwetting and antifouling Janus membranes for water reclamation from challenging industrial wastewaters through MD.

Lay Summary

Water-repellent (hydrophobic) porous membranes are commonly used in membrane distillation (MD), a desalination technology that can be used for water reclamation from highly saline water sources. When treating complex waste streams, such as oil- and gas-produced waters, however, conventional hydrophobic membranes are easily wetted and contaminated by foulants (i.e., pore wetting and membrane fouling) leading to a catastrophic failure in water recovery. In this study, we develop a novel membrane (called Janus membrane) comprising both antiwetting layer and antifouling layer. Using the Janus membrane, we successfully demonstrate in MD experiments stable water recovery and complete salt rejection, from a crude-oil-in-saline water (1 M NaCl) emulsion that mimics oil- and gas-produced water. Our study proves the great potential of antiwetting and antifouling Janus membranes for expanding the applicability of MD for water reclamation from challenging industrial wastewaters.

Preface

The research is mainly conducted in UBC's Environmental Laboratory by the author, Chenxi Li, and Dr. Xuesong Li, under the supervision of Dr. Jongho Lee, in collaboration with Xuewei Du and Dr. Tiezheng Tong from Colorado State University, and Dr. Tzahi Y. Cath from Colorado School of Mines. A version of Chapter 1-4 has been recently published¹:

Li, C.; Li, X.; Du, X.; Tong, T.; Cath, T. Y.; Lee, J. Antiwetting and Antifouling Janus Membrane for Desalination of Saline Oily Wastewater by Membrane Distillation. *ACS Applied Materials & Interfaces* **2019**, *11*, 18456–18465.

- **Li, C.**, Li, X., and Lee, J. designed the experiments.
- **Li, C.** and Li, X. conducted all of the experiments except Du, X. performed the contact angle measurements.
- **Li, C.** processed and analyzed all of the data, and all authors discussed the processed data.
- **Li, C.**, Li, X., and Lee, J. wrote the manuscript.

Table of Contents

Abstract.....	iii
Lay Summary	iv
Preface.....	v
Table of Contents	vi
List of Figures.....	vii
List of Abbreviations.....	x
List of Symbols	xi
Acknowledgements	xii
Dedication	xiii
1. Introduction	1
1.1. Background	1
1.2. Literature Review	1
1.3. Research Objectives.....	3
2. Materials and Methods	4
2.1. Materials and chemicals.....	4
2.2. Fabrication of Hydrophobic, Omniphobic, and Janus Membranes	5
2.3. Membrane Characterization	7
2.4. DCMD Experiments of Fabricated Membranes.....	8
3. Results and Discussion	11
3.1. Membrane Morphology	11
3.2. Membrane Characteristics	12
3.3. Membrane Surface Wettability	17
3.4. Membrane Wetting Resistance in Membrane Distillation	19
3.5. Membrane Fouling Resistance in Membrane Distillation	21
4. Conclusion	26
References	27

List of Figures

Figure 2.1 Fiber diameter distributions of pristine quartz fiber (QF) membranes, with an average diameter (d_{avg}) of 665.7 ± 361.8 nm.	4
Figure 2.2 Schematic illustration of the omniphobic (OMNI QF) membrane fabrication and Janus (JANUS QF) membrane fabrication by grafting a zwitterionic polymer brush layer on the omniphobic substrate (OMNI QF). (1) Imparting positive charges on quartz fiber (QF) membranes through functionalization of quartz fibers with APTES. (2) Attachment of negatively charged SiNPs to APTES-functionalized fibers via electrostatic attraction. (3) Dip-coating of the fibers in a PVDF-HFP/DMF solution blended with FDTES, producing an OMNI QF membrane. (4) Surface activation of the OMNI QF membrane via oxygen plasma. (5) Grafting of zwitterionic polymer brush layer (PSBMA) on the activated surface of the OMNI QF membrane via ATRP (JANUS QF membrane). APTES stands for (3-aminopropyl)triethoxysilane; PVDF-HFP stands for poly(vinylidene fluoride-co-hexafluoropropylene); FDTES stands for 1H,1H,2H,2H-Perfluorodecyltriethoxysilane; and SBMA stands for [2-(methacryloyloxy)-ethyl]dimethyl-(3-sulfopropyl) ammonium hydroxide.....	7
Figure 2.3 Schematic illustration of the system of DCMD experiment.	9
Figure 2.4 Size distribution of crude oil droplets in the surfactant-stabilized crude-oil-in-saline water emulsion determined from laser diffraction analysis.	10
Figure 3.1 SEM micrographs of (a) pristine QF, (b) SiNP-attached QF, and (c) OMNI QF membranes. SEM micrographs of the top (modified with PSBMA) surfaces of JANUS QF membranes fabricated from (d) 0.5 hour, (e) 1 hour, and (f) 2 hours of the ATRP reaction, with high-magnification images shown in the inserts. SEM micrographs of the bottom (unmodified) surface of JANUS QF membranes fabricated from (g) 0.5 hour, (h) 1 hour, and (i) 2 hours of the ATRP reaction.	12
Figure 3.2 ATR-FTIR spectra of the OMNI QF and JANUS QF membranes (left) with magnified views of the spectra of ester and sulfonate groups (right).	13
Figure 3.3 EDS spectrum of the thin film (PSBMA) on the top (modified) surface of the JANUS QF-2h membrane.	13

Figure 3.4 Thickness of the PSBMA film with different durations of the ATRP reaction. PSBMA brushes were grafted onto a clean glass slide on which a PVDF-HFP film was cast first by a glass rod.	14
Figure 3.5 Water contact angles on the OMNI QF membrane and the top surface (PSBMA layer grafted) of the JANUS QF membranes. Error bars represent the standard deviations of contact angle measurements for at least three different membrane samples (both left and right contact angles were measured on each sample).	15
Figure 3.6 (a) Dark-field image and (b) fluorescence image of the cross-section of the Rhodamine B-stained JANUS QF-2h membrane. The dark-field image showed the whole cross-section of the membrane, while the bright zone in the fluorescence image indicated the hydrophilic PSBMA layer.	16
Figure 3.7 Fluorescence microscopy images of the cross-sections of OMNI QF membranes treated with oxygen plasma for (a) 1 minute, (b) 3 minutes, and (c) 5 minutes at 60 mTorr, followed by their contact to a Rhodamine B (0.2 mM) solution in ethanol....	16
Figure 3.8 Contact angles of four different testing liquids (water, crude oil, hexadecane, and ethanol) on the surface of the hydrophobic QF and OMNI QF membranes. “Wicking” represents that the membrane was wetted by the testing liquid droplet and no stable contact angle could be measured. Error bars represent the standard deviations of contact angle measurements for at least three different membrane samples (both left and right contact angles were measured on each sample).	17
Figure 3.9 Photographs of liquid droplets placed on different membrane surfaces (hydrophobic, omniphobic, and hydrophilic).	18
Figure 3.10 Fluorescence microscopy image of the cross-section of the JANUS QF-2h membrane after the membrane was brought in contact with a Rhodamine B (0.2 mM) solution in ethanol.	19
Figure 3.11 Time traces of normalized water flux, J/J_0 , and salt rejection of the hydrophobic QF (square symbols) and OMNI QF (circle symbols) membranes using 1 M NaCl solution at 60 °C with different SDS concentrations as the feed solutions and deionized water at 20 °C as the permeate solution. Surface tensions of the feed streams based on the sequential doses of SDS are also indicated. The initial water fluxes (J_0) of the hydrophobic QF and OMNI QF membranes were 28.6 ± 1.5 and $19.0 \pm 1.9 \text{ L m}^{-2} \text{ h}^{-1}$, respectively.	20

Figure 3.12 Long-term wetting resistance tests of the OMNI QF (circle symbols) and JANUS QF-2h (diamond symbols) membranes for DCMD using 1 M NaCl solution with 0.2 mM SDS at 60 °C as the feed solution and deionized water at 20 °C as the permeate solution.....	21
Figure 3.13 Effects of membrane surface wettability on the oil-repelling property. Snap shots of crude oil droplets on the OMNI QF membrane (a) before and (b) after immersion in water, and on the JANUS QF-2h membrane (c) before and (d) after immersion in water.....	22
Figure 3.14 Underwater oil contact angles on (a) the OMNI QF membrane and (b) the top surface (PSBMA layer grafted surface) of the JANUS QF-2h membrane.	22
Figure 3.15 Comparison of wetting and fouling behaviors of the hydrophobic QF, OMNI QF, and JANUS QF-0.5h membranes in DCMD tests using a saline oil-in-water emulsion containing 1 M NaCl, 0.5 g L ⁻¹ crude oil, and 0.03 g L ⁻¹ TWEEN 20 at 60 °C as the feed solution and deionized water at 20 °C as the permeate solution. (a) Normalized water flux, J/J_o , and permeate conductivity of the hydrophobic QF (square symbols) and OMNI QF (circle symbols) membranes, where the hydrophobic QF membrane exhibits poor wetting resistance. (b) Normalized water flux, J/J_o , and permeate conductivity of the OMNI QF (circle symbols) and JANUS QF-0.5h (square symbols) membranes. The flux decline for both membranes with comparable rates indicates a similar fouling propensity. The rapid increase of conductivity after approximately 240 minutes indicates pore wetting. The initial water fluxes (J_o) of the hydrophobic QF, OMNI QF, and JANUS QF-0.5h membranes were 26.3 ± 0.4 , 15.8 ± 1.5 , and 18.4 ± 0.8 L m ⁻² h ⁻¹ , respectively.....	24
Figure 3.16 Time traces of normalized water flux, J/J_o , and permeate conductivity of the OMNI QF (circle symbols), JANUS QF-1h (triangle symbols), and JANUS QF-2h (diamond symbols) membranes using a saline oil-in-water emulsion containing 1 M NaCl, 0.5 g L ⁻¹ crude oil, and 0.03 g L ⁻¹ TWEEN 20 at 60 °C as the feed solution and deionized water at 20 °C as the permeate solution. The initial water fluxes (J_o) of the OMNI QF, JANUS QF-1h, and JANUS QF-2h membranes were 15.8 ± 1.5 , 17.5 ± 1.5 , and 15.5 ± 0.3 L m ⁻² h ⁻¹ , respectively.....	24

List of Abbreviations

APTES	(3-aminopropyl) triethoxysilane
ATRP	Atom-transfer radical-polymerization
ATR-FTIR	Attenuated total reflectance–Fourier-transform infrared spectroscopy
DCMD	Direct-contact membrane distillation
DI	Deionized
DMF	N,N-dimethylformamide
EDS	Energy-dispersive X-ray spectroscopy
FDTES	1H,1H,2H,2H-Perfluorodecyltriethoxysilane
IPA	Isopropanol
MD	Membrane distillation
NaCl	Sodium chloride
OMNI	Omniphobic
PEG	Polyethylene glycol
PSBMA	Zwitterionic polymer, poly(SBMA)
PVDF-HFP	Poly(vinylidene fluoride-co-hexafluoropropylene)
QF	Quartz fiber
RF	Radio frequency
RO	Reverse osmosis
SBMA	[2-(methacryloyloxy)-ethyl]dimethyl-(3-sulfopropyl)ammonium hydroxide
SDS	Sodium dodecyl sulfate
SEM	Scanning electron microscope
SiNP(s)	Silica nanoparticle(s)
TEOS	Tetraethoxysilane
TPMA	Tris(2-pyridylmethyl)amine
TWEEN 20	Polyoxyethylenesorbitan monolaurate

List of Symbols

A_m	Effective membrane area (m^2)
C_F	Salt concentration in the feed (mol L^{-1})
C_P	Salt concentration in the permeate (mol L^{-1})
J_w	Water flux ($\text{L m}^{-2} \text{ h}^{-1}$)
J_o	Initial water flux ($\text{L m}^{-2} \text{ h}^{-1}$)
Δm_p	Mass change in the permeate during the time period of Δt (kg)
ρ	Water density (kg m^{-3})
R	Salt (NaCl) rejection (%)
Δt	Time interval (h)
V_P	Total permeate volume (L)
γ	Surface tension (mN m^{-1})

Acknowledgements

This research project is conducted with the help and guidance from many respected people, who deserve my greatest gratitude.

I would like to express my deepest gratitude toward my supervisor Dr. Jongho Lee for his constant encouragement and support throughout my MASc study. His persistent patience, scientific guidance and innovative ideas enable me to acquire continuous growth and complete the research.

I would like to thank Dr. Xuesong Li for his valuable suggestions, continuous support, and great contribution to this project.

I would also like to acknowledge Xuewei Du, Dr. Tiezheng Tong, and Dr. Tzahi Y. Cath for their help.

I sincerely appreciate the help from Otman Abida, Scott Jackson, and Simon Lee in the buildup of experimental setup.

Last but not least, special thanks go to my parents for their support and dedication.

To myself

To my family

1. Introduction

1.1. Background

With the increase in water demand, water reclamation and reuse have become a desirable practice in the water supply industry.² Following the agricultural sector, industries are the second largest consumers of fresh water, withdrawing approximately 20 % of fresh water in the world.³ In particular, the oil and gas industry consumes large volumes of water during exploration of shale oil and gas and generates large volumes of wastewater, referred to as produced water, having a complex chemical composition and being highly saline (up to 360,000 mg L⁻¹).^{4,5} Membrane separation processes such as reverse osmosis (RO) are the state-of-the-art technology for desalination;⁶ however, RO is often inadequate for treating the produced water, as the salinity limit of feedwater for RO applications is approximately 70,000 mg L⁻¹, due to the high osmotic pressure that needs to be overcome by the process.⁷⁻⁹ An emerging membrane technology, membrane distillation (MD), is a promising alternative for treating such highly saline wastewaters.^{10,11}

1.2. Literature Review

MD is a desalination technology that can be used to reclaim water from highly saline streams. In a direct-contact MD (DCMD), the most commonly used configuration of MD, a hydrophobic microporous membrane keeps the hot feedwater and cold permeate (distillate) water separated, allowing only gas species (not liquid) to pass through the membrane and rejecting nonvolatile species (e.g., salts).^{10,11} The temperature difference between the feed and permeate creates a water vapor pressure gradient across the membrane pores, driving water vapor from the hot (feed) side to the cold (permeate) side of the membrane pores. MD has several advantages over conventional membrane desalination processes, including the high salt rejection, water flux nearly independent of feed salinity, and relatively low temperature requirement (40 – 70 °C) of the feedwater, which allows for the utilization of low-grade heat sources.^{12,13}

Despite these advantages, membrane wetting and fouling remain major challenges for MD.¹⁰ Mitigation of these two phenomena (i.e., pore wetting and membrane fouling) requires conflicting surface properties. Conventional hydrophobic membranes are prone to pore wetting

by a feed solution with reduced surface tensions, which can be caused by surfactants frequently found in the produced water.¹⁴ Accordingly, recent studies have demonstrated that omniphobic membranes exhibit extreme wetting resistance against both surfactant-containing water and low-surface-tension organic solvents.¹⁴⁻¹⁶ In contrast, fouling resistance to organic pollutants, such as oil and grease found in produced water,^{17,18} generally requires a hydrophilic membrane surface.¹⁹⁻²³ Thus, an ideal MD membrane used for the treatment of complex waste streams needs to possess both hydrophilic and omniphobic surface properties.

Fabrications of MD membranes that have such disparate surface wettabilities (called Janus membranes) have been recently investigated. In most cases, hydrophobic porous substrates were modified through the deposition of hydrophilic materials, such as polyethylene glycol,¹⁹ polydopamine,^{22,24-27} hydrogel,^{23,28} inorganic/composite particles,^{19,20} and electrospun hydrophilic polymers,²¹ or through creating hydrophilic functional groups.²⁹ While hydrophilic surface modification using an omniphobic substrate has also been investigated,²¹ the liquid-repelling nature of the omniphobic substrate makes it difficult to apply conventional solvent-based hydrophilic modifications. In addition, the conflicting wettabilities of the hydrophilic layer and the omniphobic layer may cause delamination if a robust bonding between the two parts is absent. Therefore, integrating the two layers through covalent bonding is desirable for membrane integrity in a long-term operation.¹⁹

As antifouling materials, zwitterionic polymers have been receiving increasing attention because of their exceptional hydrophilicity.³⁰⁻³² Comprising both cationic and anionic functional groups, zwitterionic polymers attain a high degree of hydration, effectively preventing surface adsorption of organic pollutants, even more effective than commonly used ethylene glycol-based polymers such as polyethylene glycol (PEG).³³⁻³⁶ However, zwitterionic polymers have not been investigated in the fabrication of antifouling Janus membranes for MD applications. Integrating the exceptionally fouling-resistant zwitterionic polymers and highly wetting-resistant omniphobic substrates through robust chemical bonding will likely maximize the utility of the two materials for the development of long-term, reliable MD process for challenging industrial wastewater treatment.

1.3. Research Objectives

In this work, we aim to develop a Janus membrane that simultaneously possesses wetting and fouling resistances for treating saline oily wastewaters through MD by creating a thin hydrophilic layer on an omniphobic substrate. Our main research objectives are described as follows:

1. Fabrication of a porous substrate which is not only hydrophobic but also oleophobic (i.e., omniphobic) for the Janus membrane to acquire an excellent wetting resistance. The omniphobicity of the substrate can be achieved by constructing a multilevel re-entrant structure, followed with a surface modification with low-surface-energy materials.
2. Creation of a fouling-resistant hydrophilic layer on the omniphobic substrate by grafting a zwitterionic polymer layer on the substrate through a surface-initiated atom-transfer radical-polymerization (ATRP) process.
3. Grafting of the hydrophilic layer with a controlled thickness on the top surface of the omniphobic substrate for minimization of its impact on the bulk omniphobicity, water vapor flux, and salt rejection.
4. Demonstration of stable desalination of saline oily feedwater using the Janus membrane. Specifically, we aim to demonstrate stable water flux and complete salt rejection from oil-in-saline water emulsion that mimics a challenging wastewater from oil- and gas-industry.

2. Materials and Methods

2.1. Materials and chemicals

Quartz fiber (QF) membranes (type: QR-100) with an average thickness of 0.38 mm were supplied by Sterlitech (Kent, WA). The QF membrane retains 99.99% of dioctylphthalate-derived particles with the diameter of 0.3 μm (data from the supplier), and its porosity is $79.3 \pm 1.3\%$ determined by the pycnometric method.³⁷ The average fiber diameter (d_{avg}) of the QF membrane is 665.7 ± 361.8 nm (Figure 2.1). Tetraethoxysilane (TEOS, 99.9%, Alfa Aesar), ammonium hydroxide solution (28-30%, VWR International), and ethanol ($\geq 99.9\%$, Electron Microscopy Sciences) were used for the preparation of silica nanoparticles (SiNPs). 1H,1H,2H,2H-Perfluorodecyltriethoxysilane (FDTES, 98%) was purchased from Gelest Inc. N,N-dimethylformamide (DMF, 99.8%) was acquired from VWR International. [2-(methacryloyloxy)-ethyl]dimethyl-(3-sulfopropyl)ammonium hydroxide (SBMA, 95%) was received from Toronto Research Chemicals. Hexane ($\geq 98.5\%$), hexadecane ($\geq 98\%$), sodium chloride (NaCl, $\geq 99\%$), and polyoxyethylenesorbitan monolaurate (TWEEN 20) were obtained from Fisher Scientific. Sodium dodecyl sulfate (SDS, Fisher Scientific) and light naphthenic crude oil (ONTA) were selected as the amphiphilic surfactant and oil foulant for the antiwetting and antifouling tests of MD, respectively. Deionized water was produced by a Synergy[®] UV water purification system (Millipore, Billerica, MA). The other chemicals were purchased from Sigma-Aldrich unless otherwise stated.

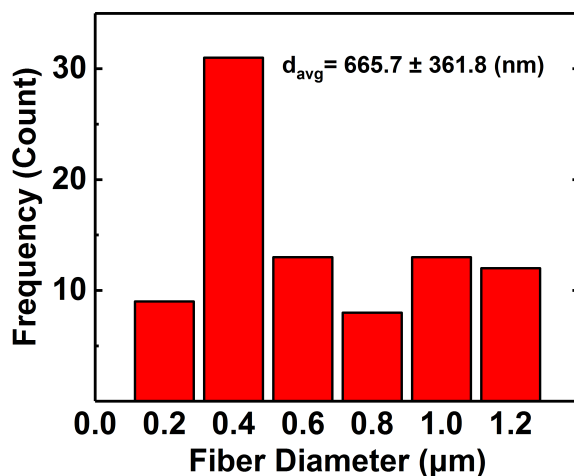


Figure 2.1 Fiber diameter distributions of pristine quartz fiber (QF) membranes, with an average diameter (d_{avg}) of 665.7 ± 361.8 nm.

2.2. Fabrication of Hydrophobic, Omniphobic, and Janus Membranes

SiNPs with a relatively monodispersed size distribution (~150 nm) were first prepared by the Stöber method.³⁸ Briefly, 13.5 mL of TEOS was added into 136.5 mL of ethanol and then stirred for 10 minutes. The solution was subsequently added to a well-mixed solution of 6 mL of ammonium hydroxide, 48.6 mL of ethanol, and 95.4 mL of deionized water. The mixture kept being stirred for 2 hours at 30 °C. After stirring, the suspension was diluted with deionized water, and SiNPs were recovered by centrifuging the suspension at 7,000 rpm for 0.5 hour. The recovered SiNPs were rinsed with deionized water several times and then dispersed in acetate buffer (0.01M, pH 4.0), resulting in a SiNP suspension with the concentration of 0.026 wt%.

The fabrication process of the omniphobic (OMNI QF) and Janus (JANUS QF) membranes is illustrated in Figure 2.2. For OMNI QF membrane fabrication, a pristine QF membrane was immersed into toluene with 1% v/v (3-aminopropyl) triethoxysilane (APTES) for 3 hours under continuous shaking. The membrane was then rinsed twice with toluene and then dried in an oven at 105 °C for 5 hours to remove residual toluene and to enhance the hydrolytic stability of APTES.³⁹ The APTES-modified QF membrane was then immersed in the SiNP suspension for 15 minutes, allowing the negatively charged SiNPs to be attached onto the positively charged APTES-functionalized fibers via the electrostatic attraction force. The SiNP-attached QF membrane was gently rinsed with deionized water and then dried in an oven at 105 °C for 5 hours. Next, the fully dehydrated QF membrane was dip-coated in a DMF solution containing 3.5 wt% poly(vinylidene fluoride-co-hexafluoropropylene) (PVDF-HFP, $M_w \sim 400,000$) and 1% v/v FDTES, which was subsequently placed in an oven at 105 °C to completely remove DMF. A hydrophobic QF membrane was fabricated by the same protocol except that FDTES, the low-surface-energy additive, was absent in the PVDF-HFP/DMF solution. All fabricated hydrophobic QF and OMNI QF membranes were pressed under 0.5 bar at 160 °C for 1 hour to improve the compactness of the nanofiber membranes.⁴⁰

The fabrication of JANUS QF membranes was completed by grafting a thin layer of zwitterionic polymer (i.e., PSBMA) brushes onto the omniphobic substrate via surface-initiated ATRP, adapting the protocol in previous publications.^{41,42} We note that although initiation sites can be created by activating C-F bonds in fluorocarbon materials,^{32,43-45} the activation requires a relatively high temperature (~80 – 90 °C) due to the high C-F bond energy (~486 kJ mol⁻¹).^{43,45}

In addition, the liquid-repelling nature of the omniphobic substrate does not allow for effective generation of initiation sites via solvent-based surface modification. Instead, it was reported that abundant initiation sites for ATRP can be generated on PVDF by plasma treatment.⁴⁶ Following this protocol, the top surface of the OMNI QF membrane was activated with oxygen plasma (PE-50 plasma cleaner, Plasma Etch, Inc.) with the radio frequency (RF) power of 400 W at 60 mTorr for 1 minute. The effectiveness of plasma treatment for polymer grafting via ATRP is discussed in the following section. The plasma-treated membrane was then placed in a glass container with the activated surface facing an isopropanol (IPA) /deionized water (1:1, v/v) mixture solution (50 mL) that contains 7 mmol (1.955 g) of SBMA. Subsequently, 2 mL of Cu(II)/TPMA catalyst solution, which was prepared by dissolving copper (II) chloride (7.4 μ mol, 1 mg) and tris(2-pyridylmethyl)amine (TPMA, 48.2 μ mol, 14 mg) in 50% v/v IPA aqueous solution (2 mL), was injected into the container. The polymerization was then initiated by adding 3 mL of L-ascorbic acid solution (1 g per 10 mL of 50% v/v IPA solution) to the container. All solutions were purged with nitrogen gas before the ATRP reaction, and the entire ATRP process was conducted in a nearly oxygen-free environment shielded from light. After a designated duration of polymerization (0.5 hour, 1 hour, or 2 hours), air was introduced to terminate the ATRP reaction.⁴⁷ The modified membrane was rinsed thoroughly with 50% v/v IPA solution, followed by a rinse with deionized water.

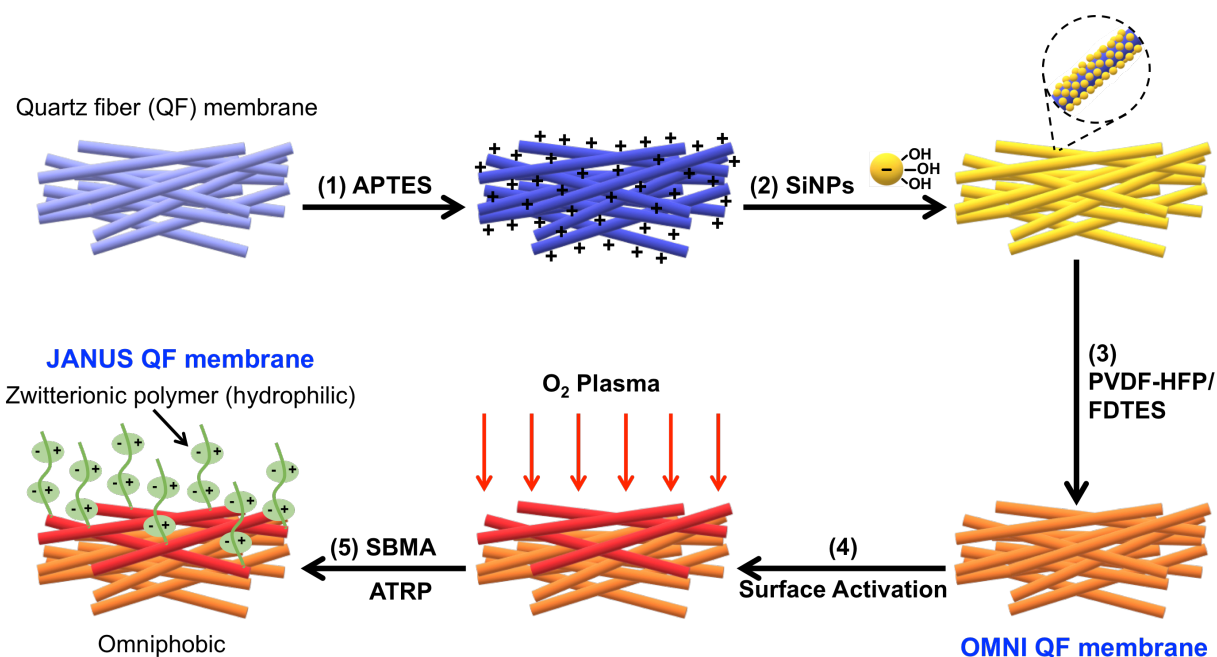


Figure 2.2 Schematic illustration of the omniphobic (OMNI QF) membrane fabrication and Janus (JANUS QF) membrane fabrication by grafting a zwitterionic polymer brush layer on the omniphobic substrate (OMNI QF). (1) Imparting positive charges on quartz fiber (QF) membranes through functionalization of quartz fibers with APTES. (2) Attachment of negatively charged SiNPs to APTES-functionalized fibers via electrostatic attraction. (3) Dip-coating of the fibers in a PVDF-HFP/DMF solution blended with FDTS, producing an OMNI QF membrane. (4) Surface activation of the OMNI QF membrane via oxygen plasma. (5) Grafting of zwitterionic polymer brush layer (PSBMA) on the activated surface of the OMNI QF membrane via ATRP (JANUS QF membrane). APTES stands for (3-aminopropyl)triethoxysilane; PVDF-HFP stands for poly(vinylidene fluoride-co-hexafluoropropylene); FDTS stands for 1H,1H,2H,2H-Perfluorodecyltriethoxysilane; and SBMA stands for [2-(methacryloyloxy)-ethyl]dimethyl-(3-sulfopropyl) ammonium hydroxide.

2.3. Membrane Characterization

The surface morphology and elemental information on the fabricated membranes were examined using a scanning electron microscope (SEM, FEI Qanta 650) equipped with an X-ray detector for energy-dispersive X-ray spectroscopy (EDS, Oxford instrument). The functional groups of the fabricated membranes were qualitatively investigated by attenuated total reflectance–Fourier-transform infrared spectroscopy (ATR-FTIR, Perkin-Elmer Frontier FTIR with universal ATR accessory) over the scan range 650 – 4000 cm^{-1} . Surface wettability of the fabricated membranes was assessed by measurements of the contact angles of different liquids using a goniometer

(Ramé-Hart 200-F1). In addition, the wetting of the zwitterionic polymer layer on the JANUS QF membrane was visualized by an inverted epifluorescence microscope (Nikon[®] Eclipse[™] TE2000-U) equipped with a CMOS camera (LaVision). Specifically, a JANUS QF-2h membrane was first soaked in an aqueous solution containing 0.2 mM Rhodamine B for 10 minutes. After the excess solution on the membrane surface was gently wiped out using clean tissues, the membrane sample was visualized under the microscope with an excitation wavelength of 529 – 535 nm.

The thickness of the PSBMA film with different durations of polymerization was measured by a profilometer (DekakXT, Bruker). Since it is challenging to directly measure the thickness of the PSBMA brush layer on a fiber mat, a PVDF-HFP film was cast from a solution of 3.5 wt% PVDF-HFP in DMF on a 7.5 cm × 3.8 cm clean glass slide using a glass rod. The top surface of the cast film was pressed with another clean glass slide and placed in an oven at 180 °C for 3 hours to minimize the roughness of the PVDF-HFP film.⁴⁸ Next, the pressed PVDF-HFP film was partially covered by a clean glass slide prior to surface activation by oxygen plasma. After plasma treatment, the glass cover was removed, and ATRP was performed by immersing the whole film in an SBMA solution for different reaction time periods (1 hour, 2 hours, and 4 hours). PSBMA was grafted only on the exposed zone to the oxygen plasma. Subsequently, the PSBMA film thickness was measured as the height difference between the plasma-exposed zone and the unexposed zone on at least three random locations using a profilometer with a 12 μm stylus tip.⁴⁹

2.4. DCMD Experiments of Fabricated Membranes

The wetting and fouling behaviors of the fabricated membranes were assessed by DCMD experiments carried out in a bench-scale MD unit with a membrane cell in a countercurrent crossflow mode (Figure 2.3). The effective membrane area was 15 cm² (6.3 cm × 2.4 cm). The temperatures of the feed and permeate streams were maintained at 60 °C and 20 °C, respectively, by using two circulating water baths (Polystat Standard, Cole-Parmer, Vernon Hills, IL). The feed was circulated at a slightly higher crossflow velocity, 5.6 cm s⁻¹, than the permeate, 3.7 cm s⁻¹, which induced a little higher pressure in the feed than in the permeate and therefore allows for unambiguous detection of membrane pore wetting.

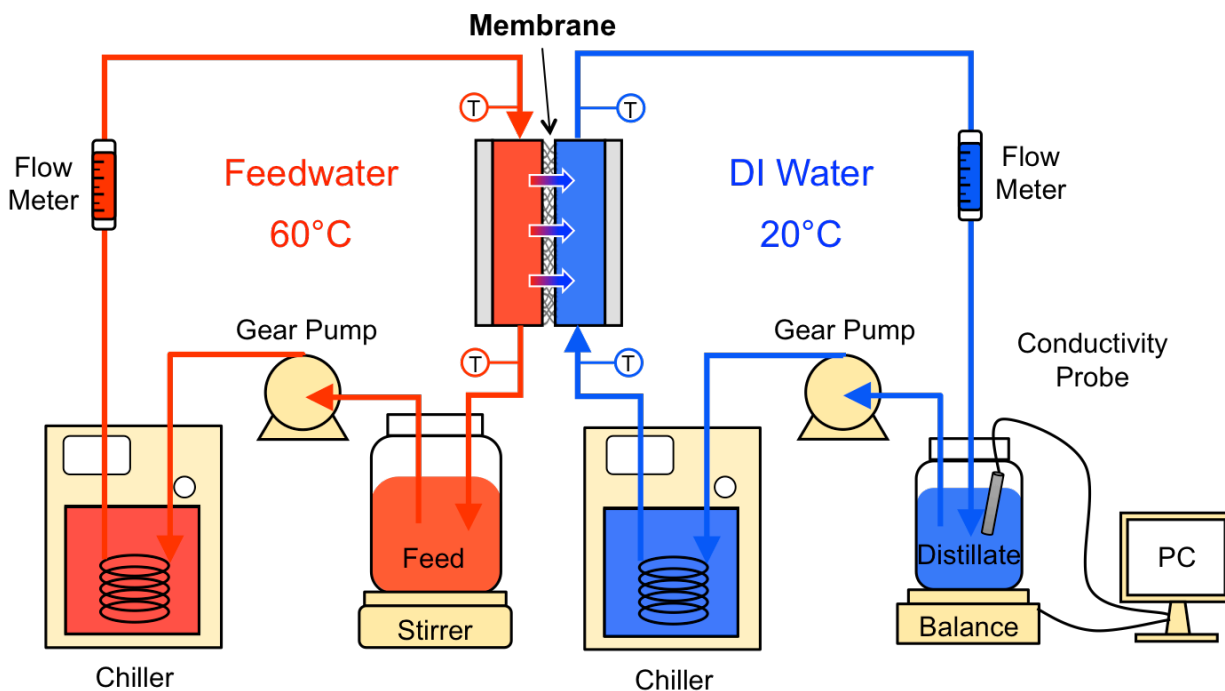


Figure 2.3 Schematic illustration of the system of DCMD experiment.

In MD wetting tests, 1 M NaCl solution and deionized water were used as the feed and permeate solutions, respectively. To investigate wetting behaviors of the fabricated membranes in the feed solution with varying surface tensions, SDS was periodically added to the feed every 2 hours. The SDS concentrations in the hot feed after the sequential additions were 0.05, 0.1, 0.15, and 0.2 mM. Consequently, the surface tensions of the feed were reduced to ~ 48 , ~ 41 , ~ 37 , and ~ 33 mN m⁻¹, respectively, from ~ 66 mN m⁻¹ of saline (1 M NaCl) water at 60 °C.⁵⁰

In MD fouling experiments, a saline crude-oil-in-water emulsion was used as the feed. The emulsion was prepared by mixing 0.5 g L⁻¹ crude oil and 0.03 g L⁻¹ TWEEN 20 with 1 M NaCl solution using a laboratory blender at 20,000 rpm for 5 minutes. This synthetic feed solution simulates the real produced water that contains salts (1,000 – 400,000 mg L⁻¹), grease and oil (2 – 560 mg L⁻¹), and surfactants.^{4,5,9} A particle size analyzer (Mastersizer 2000, Malvern) was used to acquire the size distribution of oil droplets in the emulsion (Figure 2.4). The surface volume mean diameter (i.e., D[3,2]) of the oil droplets was 0.866 μ m, and 90% of the total oil volume comprised oil droplets with diameters smaller than 3.861 μ m (i.e., D[0.9] = 3.861 μ m). For JANUS QF membranes, the PSBMA-modified surface was left to face the feed solution, while for other membranes there was no specific orientation between the two membrane sides.

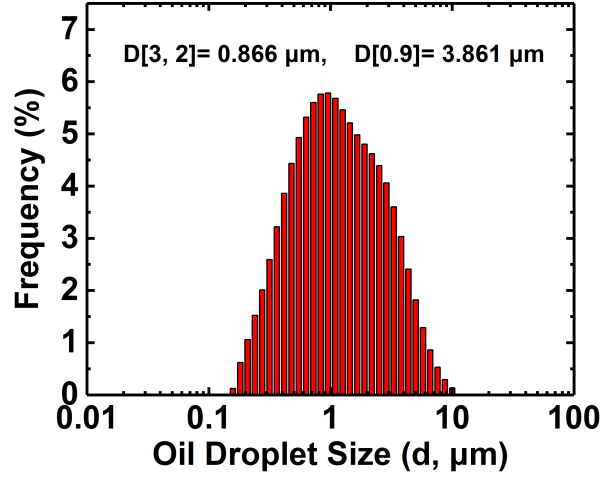


Figure 2.4 Size distribution of crude oil droplets in the surfactant-stabilized crude-oil-in-saline water emulsion determined from laser diffraction analysis.

For both wetting and fouling experiments, the weight change in the permeate was monitored by a digital balance (Symmetry 4202E PT, Cole-Parmer, Vernon Hills, IL) with an accuracy of ± 0.01 g, and the weight data was collected by WinWedge software (TALtech, PA) to determine the real-time water flux, J_w , through the membrane, using the following equation:

$$J_w = \frac{\Delta m_p}{\rho A_m \Delta t} \times 1000 \quad (1.)$$

where Δm_p (kg) is the mass change in the permeate during the time period of Δt , ρ is the water density (kg m^{-3}), A_m is the effective membrane area ($1.5 \times 10^{-4} \text{ m}^2$), and Δt is the time interval (h). The factor of 1000 was multiplied to express J_w in the unit of $\text{L m}^{-2} \text{ h}^{-1}$.

The conductivity of the permeate solution was monitored by a conductivity meter (Oakton CON 2700, Oakton Instruments, Vernon Hills, IL) with built-in software, and the conductivity meter has an accuracy of $\pm 0.1 \text{ } \mu\text{S cm}^{-1}$. The salt (NaCl) rejection, R , was calculated by using

$$R = 1 - \frac{\Delta(V_P C_P) / J_w A_m \Delta t}{C_F} \quad (2.)$$

where V_P is the total permeate volume (L), C_F and C_P are the salt concentrations in the feed and permeate (mol L^{-1}), respectively, and $\Delta(V_P C_P)$ indicates the mass of salt that passed through the membrane during the time period of Δt .

3. Results and Discussion

3.1. Membrane Morphology

SEM micrographs depicting the surface morphology of the pristine and fabricated QF membranes are shown in Figure 3.1. To achieve surface omniphobicity, re-entrant structures and low surface energy are essential.^{14,16,51} The cylindrical geometry of fibers of the pristine QF membrane features a primary re-entrant structure (Figure 3.1a), which provides a kinetic barrier against the wetting transition from the Cassie-Baxter to Wenzel state. The SiNP-attached QF membrane displays a dense deposition of spherical SiNPs having a relatively uniform size on the quartz fibers (Figure 3.1b), which establishes a multilevel re-entrant structure.^{14,52} After immersing the membrane in the PVDF-HFP/FDTES solution, a thin film was uniformly coated on the surface of the fibers and SiNPs (OMNI QF membrane, Figure 3.1c), while preserving the multilevel re-entrant structure.

The uniformly coated PVDF-HFP/FDTES film on the SiNPs and quartz fibers, followed by plasma treatment,⁴⁶ provides abundant sites onto which PSBMA brush can be grafted via surface-initiated ATRP. Figure 3.1d-f shows top surface SEM micrographs of JANUS QF membranes with different durations of the ATRP reaction. In comparison with the bottom surface (without the PSBMA brush layer, Figure 3.1g-i), the membrane pores on the top surface are partially covered by a filmlike PSBMA layer, with a larger coverage for a longer ATRP reaction time. The absence of these films at the bottom surfaces of the JANUS QF membranes (Figure 3.1g-i) indicates that the surface-initiated ATRP only occurred on the top surface due to the formation of initiation sites for ATRP via oxygen plasma treatment.

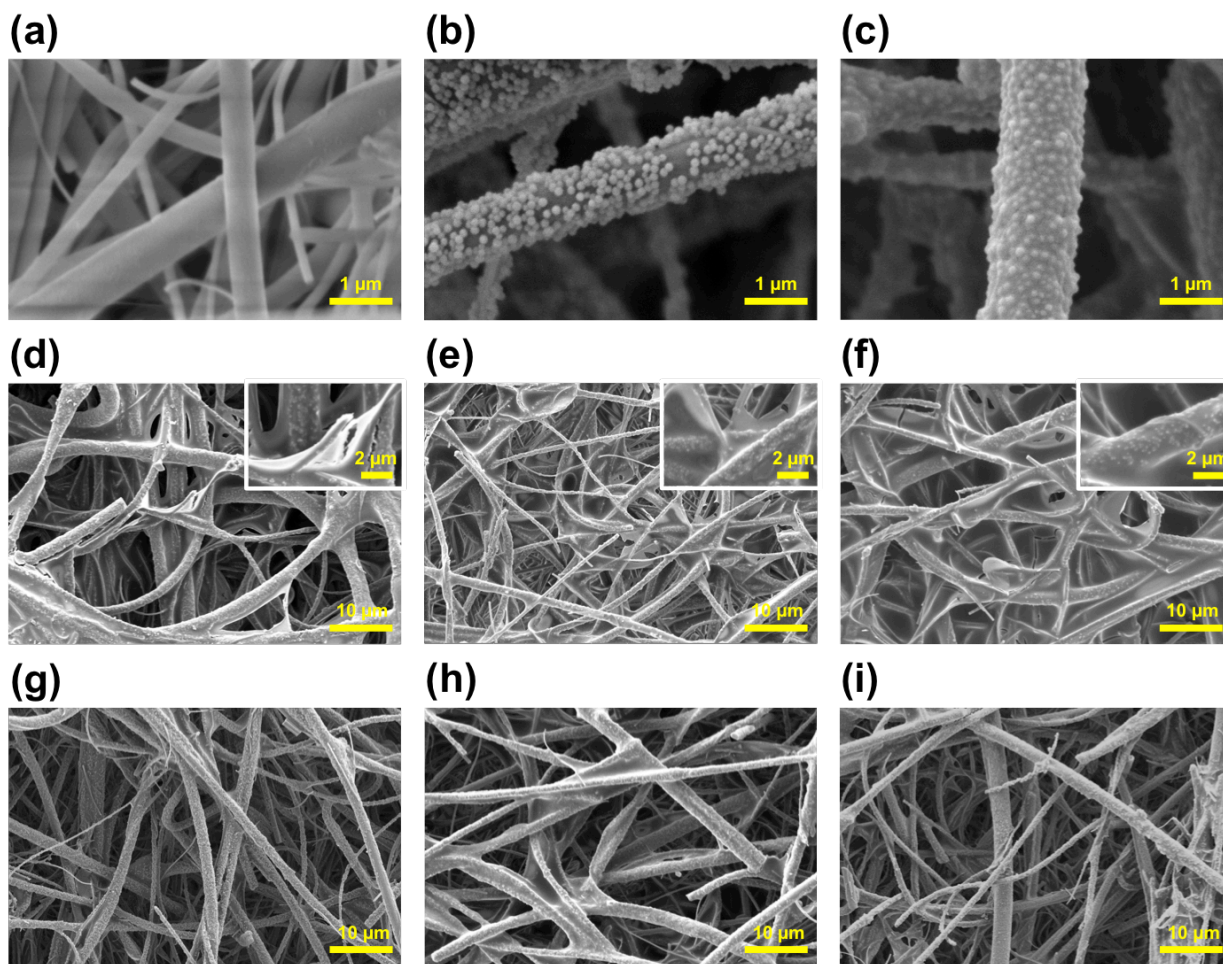


Figure 3.1 SEM micrographs of (a) pristine QF, (b) SiNP-attached QF, and (c) OMNI QF membranes. SEM micrographs of the top (modified with PSBMA) surfaces of JANUS QF membranes fabricated from (d) 0.5 hour, (e) 1 hour, and (f) 2 hours of the ATRP reaction, with high-magnification images shown in the inserts. SEM micrographs of the bottom (unmodified) surface of JANUS QF membranes fabricated from (g) 0.5 hour, (h) 1 hour, and (i) 2 hours of the ATRP reaction.

3.2. Membrane Characteristics

The characteristic functional groups of the fabricated membranes were qualitatively characterized by ATR-FTIR to verify the grafting of the PSBMA layer on the membrane surface. Figure 3.2 shows the ATR-FTIR spectra with the wavenumber range $1800\text{--}700\text{ cm}^{-1}$, which covers the characteristic infrared absorption bands of the main functional groups of the fabricated JANUS QF membranes with different durations of polymerization. By comparing the spectra of the OMNI QF and JANUS QF membranes, two additional peaks at 1726 and 1035

cm^{-1} were found in the spectra of the JANUS QF membranes only, representing two major functional groups of SBMA: the ester group and the sulfonate group, respectively.^{41,53,54} The presence of the characteristic element, sulfur, in PSBMA was also revealed via the EDS scanning of the top surface of the JANUS QF-2h membranes (Figure 3.3), demonstrating a successful grafting of PSBMA brush layers on the surface of the JANUS QF membranes.

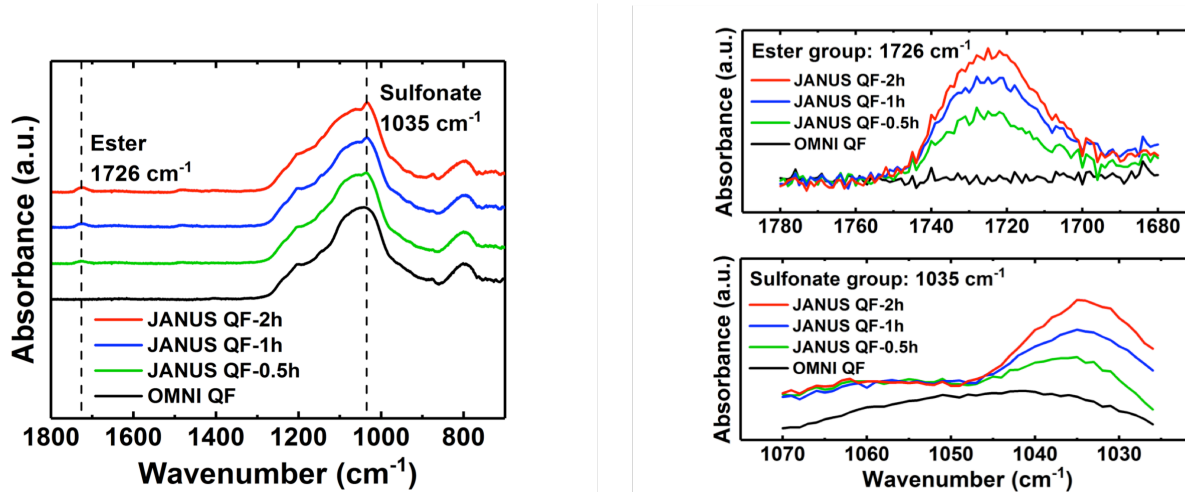


Figure 3.2 ATR-FTIR spectra of the OMNI QF and JANUS QF membranes (left) with magnified views of the spectra of ester and sulfonate groups (right).

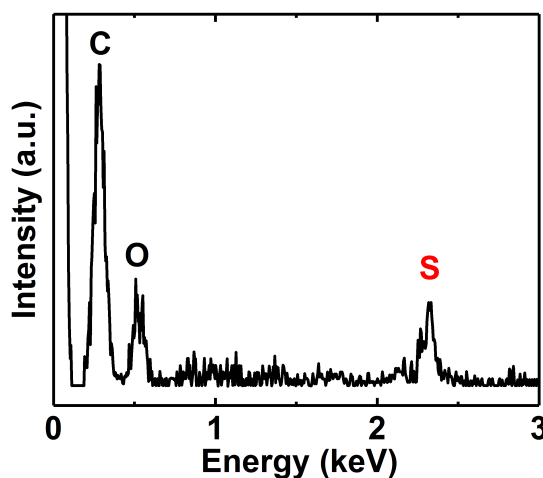


Figure 3.3 EDS spectrum of the thin film (PSBMA) on the top (modified) surface of the JANUS QF-2h membrane.

Additionally, the absorbance intensities of the ester and the sulfonate groups increase with a longer duration of the ATRP reaction (Figure 3.2), suggesting an increased amount of PSBMA. To further explore the relationship between the thickness of the PSBMA brush layer and ATRP reaction time, a PSBMA film was formed on a glass slide through the identical process for the fabrication of JANUS QF membranes (Section 2.3); a PVDF-HFP film was first cast on a glass slide, the film was exposed to oxygen plasma, and a PSBMA brush layer was grafted via ATRP with different reaction times (i.e., 1 hour, 2 hours, and 4 hours). The thickness of the brush layer increases with the reaction time (Figure 3.4), consistent with the electron microscopy (Figure 3.1d-f) and ATR-FTIR analysis (Figure 3.2). These results confirm that a precise control of the PSBMA brush layer thickness is enabled by tuning ATRP duration,^{32,55,56} consequently controlling the membranes' surface hydrophilicity and fouling resistance.

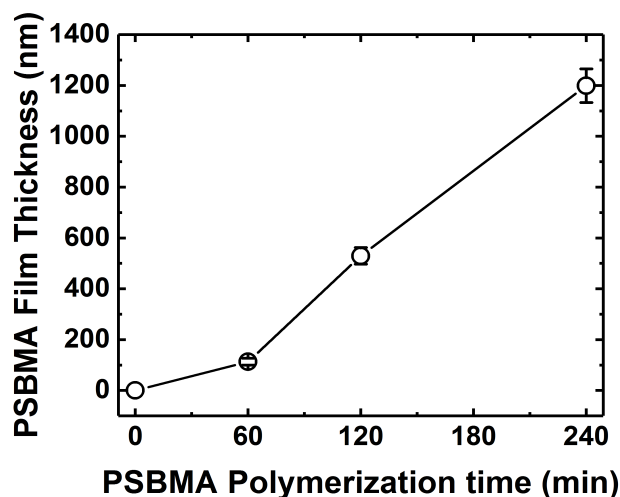


Figure 3.4 Thickness of the PSBMA film with different durations of the ATRP reaction. PSBMA brushes were grafted onto a clean glass slide on which a PVDF-HFP film was cast first by a glass rod.

Water contact angle measurements were also conducted to investigate the effects of grafted PSBMA on the surface hydrophilicity of the fabricated membranes (Figure 3.5). The PSBMA-modified surface of the JANUS QF-0.5h membrane exhibited a slightly decreased static water contact angle ($121.8^\circ \pm 3.0^\circ$) as compared to the surface of the OMNI QF membrane ($151.5^\circ \pm 4.1^\circ$). Increasing ATRP reaction time to 1 hour (JANUS QF-1h membrane) and 2 hours (JANUS QF-2h membrane) led to a further enhanced surface hydrophilicity, exhibiting progressively

reduced contact angles, $72.0^\circ \pm 4.9^\circ$ and $25.2^\circ \pm 0.5^\circ$, respectively, and showing an increased impact of the zwitterionic polymer brush on the surface hydrophilicity.

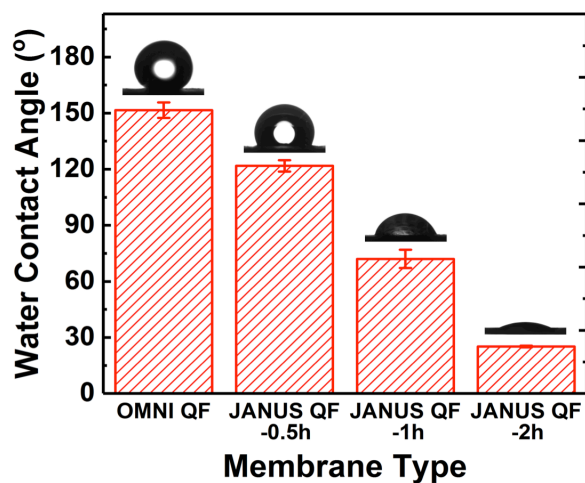


Figure 3.5 Water contact angles on the OMNI QF membrane and the top surface (PSBMA layer grafted) of the JANUS QF membranes. Error bars represent the standard deviations of contact angle measurements for at least three different membrane samples (both left and right contact angles were measured on each sample).

The presence of a thin, zwitterionic polymer layer on only one side of JANUS QF membranes was confirmed by fluorescence microscopy. After immersing the JANUS QF-2h membrane in an aqueous solution of 0.2 mM Rhodamine B, the cross-section of the membrane was imaged using a fluorescence microscope. Compared to the dark-field microscopy image (Figure 3.6a), the appearance of the thin bright strip in the fluorescence image (Figure 3.6b) clearly indicates that only the top surface of the JANUS QF membrane became hydrophilic due to the grafting of PSBMA brushes and was stained with the Rhodamine dye. The remaining part of the membrane was nonwetted, showing no presence of the dye. This suggests that plasma treatment was effective only on the top surface onto which PSBMA brushes were grafted via ATRP, while maintaining the antiwetting property of the omniphobic membrane. The confined effect of plasma treatment on the membrane surface is attributed to the three orders of magnitude greater mean free path ($\sim 800 \mu\text{m}$ at 60 mTorr)⁵⁷ as compared to the effective pore size of the QF membrane ($\sim 0.3 \mu\text{m}$), preventing the penetration of oxygen plasma into the inner domain of the membrane. For further verification, OMNI QF membranes were plasma-treated for 1, 3, and 5 minutes at RF power of 400W and 60 mTorr. Subsequently, droplets of a Rhodamine B (0.2

mM) solution in ethanol were dispensed on the membrane top surfaces. Fluorescence microscopy again revealed that only top surfaces were stained with the dye (Figure 3.7), indicating that the bulk parts of the membranes were not affected by the plasma treatment.

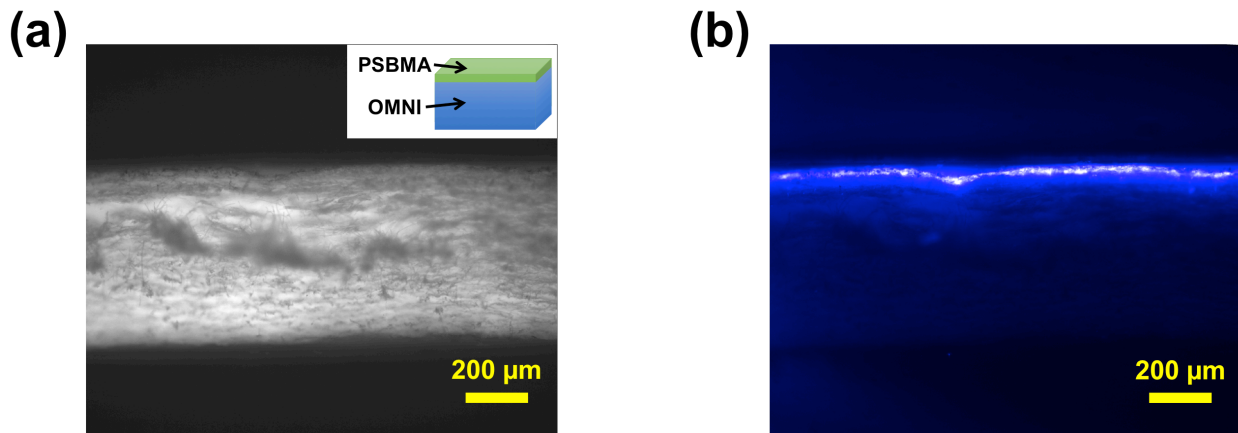


Figure 3.6 (a) Dark-field image and (b) fluorescence image of the cross-section of the Rhodamine B-stained JANUS QF-2h membrane. The dark-field image showed the whole cross-section of the membrane, while the bright zone in the fluorescence image indicated the hydrophilic PSBMA layer.

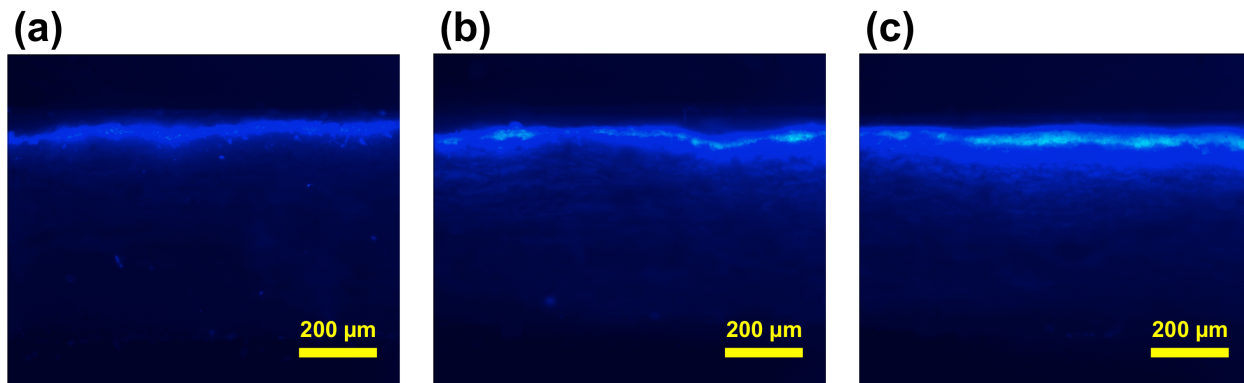


Figure 3.7 Fluorescence microscopy images of the cross-sections of OMNI QF membranes treated with oxygen plasma for (a) 1 minute, (b) 3 minutes, and (c) 5 minutes at 60 mTorr, followed by their contact to a Rhodamine B (0.2 mM) solution in ethanol.

3.3. Membrane Surface Wettability

Membrane wettability was assessed by sessile-drop contact angle measurements using several liquids with different surface tensions (γ). The testing liquids include water ($\gamma = 72 \text{ mN m}^{-1}$), crude oil ($\gamma \approx 30 \text{ mN m}^{-1}$), hexadecane ($\gamma = 27.5 \text{ mN m}^{-1}$), and ethanol ($\gamma = 22.1 \text{ mN m}^{-1}$). As shown in Figure 3.8, both hydrophobic QF and OMNI QF membranes exhibit high water contact angles, i.e., $140.6^\circ \pm 2.2^\circ$ and $151.5^\circ \pm 4.1^\circ$, respectively. Even with PVDF-HFP having a relatively high surface energy (critical surface energy $\sim 25 \text{ mN m}^{-1}$),⁵⁸ the high porosity of the fiber mat enables the hydrophobic QF membrane to attain the Cassie-Baxter state for water. However, the hydrophobic QF membrane was instantaneously wetted upon its contact with all the organic liquids. In contrast, the OMNI QF membrane retained all the liquids. The superior wetting resistance of the OMNI QF membrane can be attributed to the re-entrant structure constructed by attaching SiNPs of spherical shape to the cylindrical fibers, combined with the low surface energy of FDTES (critical surface energy $\sim 12 \text{ mN m}^{-1}$).⁵⁹

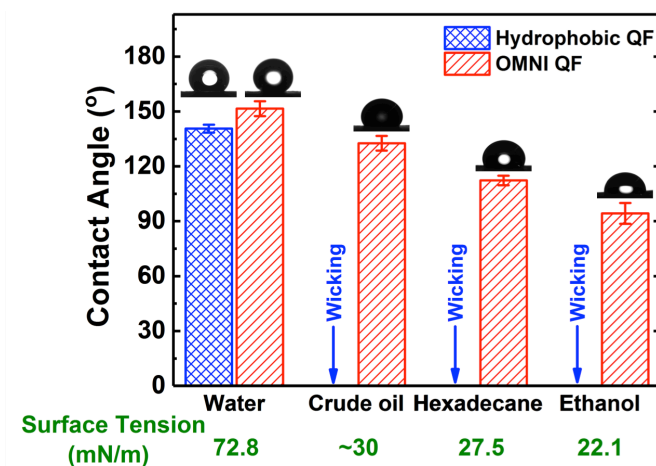


Figure 3.8 Contact angles of four different testing liquids (water, crude oil, hexadecane, and ethanol) on the surface of the hydrophobic QF and OMNI QF membranes. “Wicking” represents that the membrane was wetted by the testing liquid droplet and no stable contact angle could be measured. Error bars represent the standard deviations of contact angle measurements for at least three different membrane samples (both left and right contact angles were measured on each sample).

A visual investigation of membrane wettability was also performed by placing 10 μL liquid droplets (water, ethanol, and hexane) onto the pristine and modified membranes (Figure 3.9). As expected, all the testing liquids permeated through the entirely hydrophilic, pristine membrane. Consistent with the contact angle measurement, the hydrophobic QF membrane exhibits a high hydrophobicity but not an oleophobicity. The top surface and bottom surface of the JANUS QF-2h membrane showed distinctly different wettabilities. The bottom surface of the JANUS QF-2h membrane resisted wetting against ethanol ($\gamma = 22.1 \text{ mN m}^{-1}$) and hexane ($\gamma = 18.4 \text{ mN m}^{-1}$). On the other hand, the top surface of the JANUS QF-2h membrane became hydrophilic, and the surface was readily wetted by all the liquids. Importantly, the droplets spread over but did not permeate through the membrane, unlike the pristine membrane for all three liquids and the hydrophobic QF membrane for ethanol and hexane. This suggests that the omniphobicity exhibited by the most part of the JANUS QF membrane does not allow liquid permeation, which is critical to the use of the JANUS QF membrane in MD and also consistent with the confined presence of a hydrophilic zone observed from the cross-section images via fluorescence microscopy (Figure 3.6b and Figure 3.7). In addition, we dispensed a droplet of ethanol containing Rhodamine B (0.2 mM) on the top surface (hydrophilic side) of the JANUS QF-2h membrane. The fluorescence microscopy image of the membrane cross-section revealed that only a thin layer on the hydrophilic-side surface was stained with the fluorescence dye (Figure 3.10), which further verified the intact omniphobicity of the bulk parts of the JANUS QF membranes.

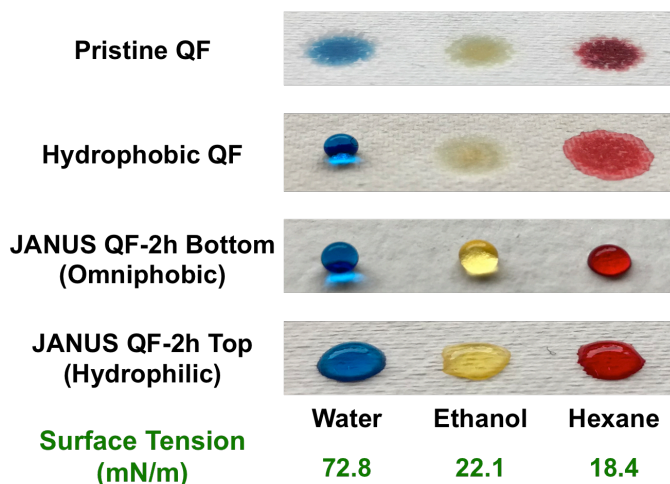


Figure 3.9 Photographs of liquid droplets placed on different membrane surfaces (hydrophobic, omniphobic, and hydrophilic).

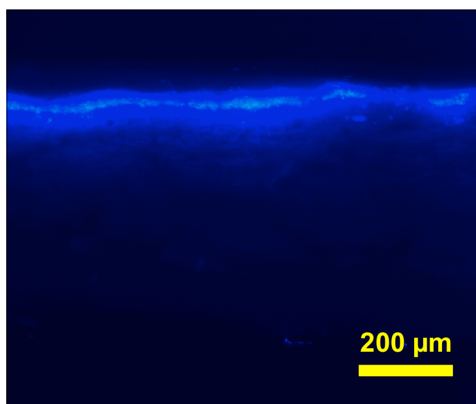


Figure 3.10 Fluorescence microscopy image of the cross-section of the JANUS QF-2h membrane after the membrane was brought in contact with a Rhodamine B (0.2 mM) solution in ethanol.

3.4. Membrane Wetting Resistance in Membrane Distillation

Maintaining a nonwetting state of the membrane is critical for a long-term, sustainable water desalination by membrane distillation (MD). We assessed wetting resistances of the hydrophobic QF, OMNI QF, and JANUS QF membranes in DCMD. Figure 3.11 shows the time traces of normalized water flux and salt rejection of the hydrophobic QF and OMNI QF membranes. Here, 1 M NaCl solution is used as feed at 60 °C and deionized water as permeate at 20 °C. Then, SDS was sequentially added into the feed every 2 hours with an increment of 0.05 mM to progressively reduce the surface tension of the feed, from $\sim 66 \text{ mN m}^{-1}$ (1 M NaCl solution) to ~ 48 , ~ 41 , ~ 37 , and $\sim 33 \text{ mN m}^{-1}$, at 0.05, 0.1, 0.15 and 0.2 mM SDS (in 1 M NaCl solution), respectively, at 60 °C. During the initial 2 hours without SDS in the feed, both membranes exhibited nearly perfect ($\sim 100\%$) salt rejections with consistent water fluxes. However, when SDS concentration in the feed was increased to 0.1 mM, the water flux of the hydrophobic QF membrane abruptly increased, and the salt rejection dropped, indicating an occurrence of pore wetting in the membrane. In contrast, the OMNI QF membrane maintained the nearly perfect salt rejection even when the surface tension was reduced to $\sim 33 \text{ mN m}^{-1}$ (0.2 mM SDS in 1M NaCl solution), demonstrating a high wetting resistance of the OMNI QF membrane.

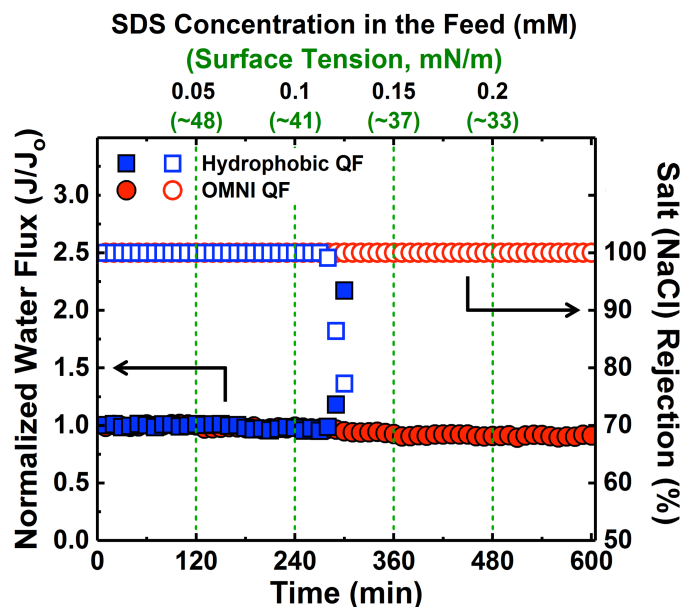


Figure 3.11 Time traces of normalized water flux, J/J_0 , and salt rejection of the hydrophobic QF (square symbols) and OMNI QF (circle symbols) membranes using 1 M NaCl solution at 60 °C with different SDS concentrations as the feed solutions and deionized water at 20 °C as the permeate solution. Surface tensions of the feed streams based on the sequential doses of SDS are also indicated. The initial water fluxes (J_0) of the hydrophobic QF and OMNI QF membranes were 28.6 ± 1.5 and 19.0 ± 1.9 L m⁻² h⁻¹, respectively.

Likewise, wetting resistances of OMNI QF and JANUS QF-2h membranes were compared in the DCMD experiments using 1 M NaCl solution as the feed at 60 °C with 0.2 mM SDS and deionized water as the permeate at 20 °C (Figure 3.12). Both membranes showed perfect salt rejections more than 30 hours, exhibiting an equally excellent wetting resistance. In particular, this experiment again confirms that the hydrophilic zwitterionic modification developed in our study does not compromise the omniphobicity of the JANUS QF membrane. We note that the water flux of the JANUS QF-2h membrane was slightly lower than that of the OMNI QF membrane, likely due to two possible mechanisms: first, the partial blockage of membrane pores by PSBMA layers (as shown in Figure 3.1d-f) could increase the vapor transport resistance; second, the water trapped in the hydrophilic PSBMA layer could result in a poor convective heat transfer and thus causes a more severe temperature polarization, leading to a compromised driving force.²⁰ Although this flux reduction is not significant, the impact of ATRP duration on the PSBMA layer thickness further allows for minimizing the flux reduction while maintaining the surface hydrophilicity.

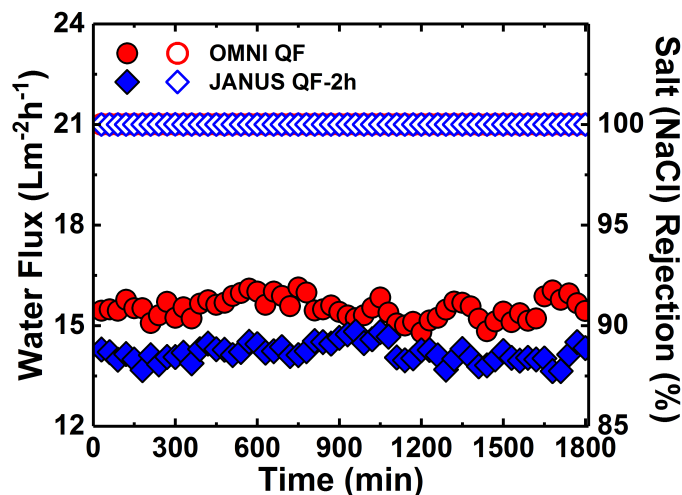


Figure 3.12 Long-term wetting resistance tests of the OMNI QF (circle symbols) and JANUS QF-2h (diamond symbols) membranes for DCMD using 1 M NaCl solution with 0.2 mM SDS at 60 °C as the feed solution and deionized water at 20 °C as the permeate solution.

3.5. Membrane Fouling Resistance in Membrane Distillation

Prior to MD experiments, a simple static fouling test was performed to examine fouling behaviors of the OMNI QF and JANUS QF membranes, using crude oil as a representative foulant in oil- and gas-produced waters. As shown in Figure 3.13a, crude oil droplets beaded up on the OMNI QF membrane surface. Upon the immersion of the membrane into water, however, these oil droplets spread and adhered onto the membrane immediately (Figure 3.13b), because of the attraction of the hydrophobic surface toward the nonpolar liquid (i.e., crude oil) over the polar liquid (i.e., water). In contrast, although the crude oil droplets spread over on the hydrophilic surface of the JANUS QF-2h membrane in air (Figure 3.13c), they were immediately detached from the membrane surface (Figure 3.13d) when the membrane was immersed in water. Consistent with these results, the OMNI QF membrane and the JANUS QF-2h membrane exhibited a low ($\sim 25.7^\circ$) and high ($\sim 152.0^\circ$) underwater-oil contact angle (Figure 3.14), respectively. This oil-repelling characteristic of the JANUS QF membrane re-emphasizes the necessity of a highly hydrophilic layer for fouling-resistant MD membranes and suggests an excellent antioil fouling property of the JANUS QF membrane, which will be further discussed in the following.

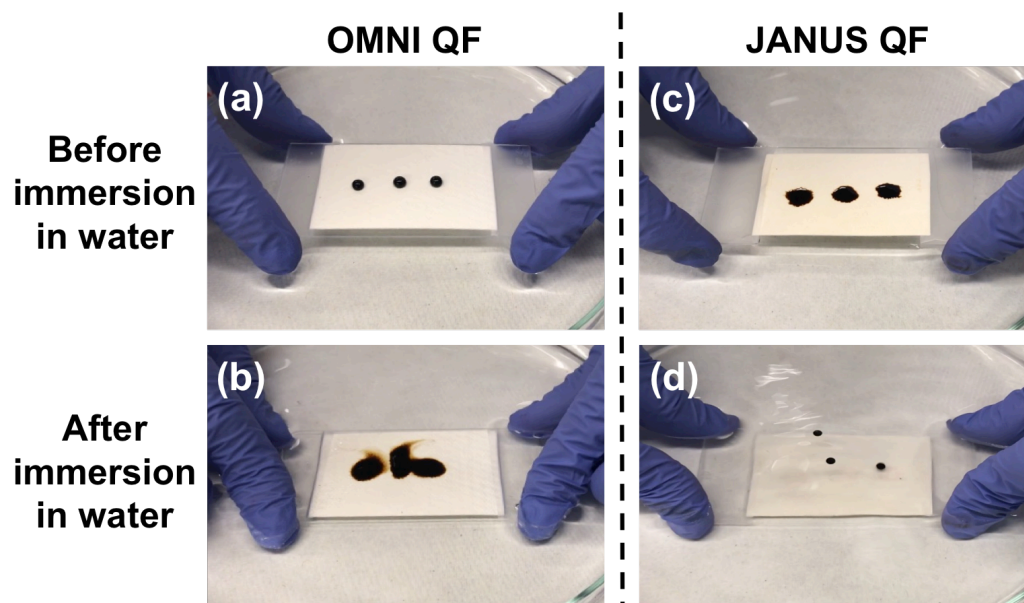


Figure 3.13 Effects of membrane surface wettability on the oil-repelling property. Snap shots of crude oil droplets on the OMNI QF membrane (a) before and (b) after immersion in water, and on the JANUS QF-2h membrane (c) before and (d) after immersion in water.

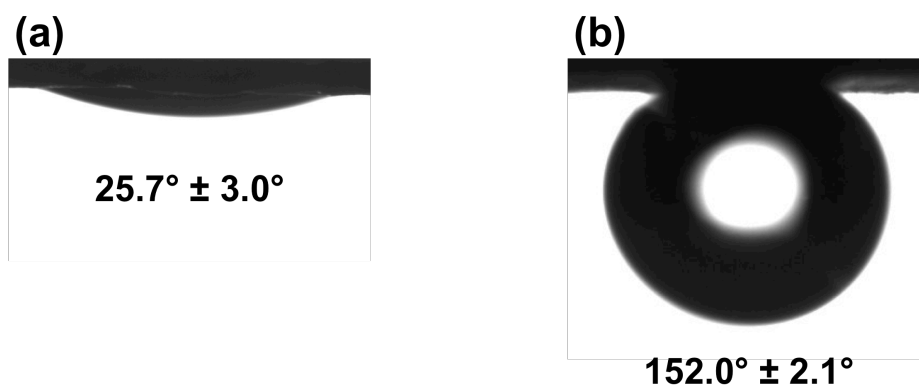


Figure 3.14 Underwater oil contact angles on (a) the OMNI QF membrane and (b) the top surface (PSBMA layer grafted surface) of the JANUS QF-2h membrane.

To investigate the antifouling performance of the JANUS QF membranes in MD, a surfactant-stabilized crude-oil-in-saline water emulsion (0.5 g L^{-1} crude oil, 0.03 g L^{-1} TWEEN 20, and 1 M NaCl) was prepared to simulate oil- and gas-produced waters. The hydrophobic QF and OMNI QF membranes were first used to examine the fouling tendency of hydrophobic and omniphobic membrane surfaces, respectively, in MD. The hydrophobic QF membrane showed rapid increases of both water flux and permeate conductivity only after a 40-min test (Figure 3.15a), indicating pore wetting and the loss of process integrity. This poor MD performance implies that conventional hydrophobic membranes are not suitable for treating oily wastewater using DCMD. The OMNI QF membrane exhibited an improved performance (Figure 3.15b), with a nearly 100% salt rejection during the first ~ 4 hours. However, the OMNI QF membrane exhibited a gradual decline of the water flux throughout the MD test, showing that the water flux reduced to an approximately 70% of the initial water flux after the initial ~ 4 hours. This continuous water flux decline suggests a severe oil fouling on the membrane surface, likely due to the nonpolar/nonpolar attraction. Moreover, the salt rejection decreased abruptly at ~ 4 hours, indicating an occurrence of membrane pore wetting of the OMNI QF membrane.

Next, JANUS QF membranes fabricated with 0.5, 1, and 2 hours of ATRP reaction times were tested. The JANUS QF-0.5h membrane showed virtually no improvement in wetting and fouling resistances compared to the OMNI QF membrane (Figure 3.15b), likely due to the insufficient coverage or thickness of the zwitterionic polymer layer. However, a further increase of ATRP reaction time led to a reduced fouling propensity. The rate of the water flux decline of the JANUS QF-1h membrane was two-fold lower than that of the OMNI QF membrane (Figure 3.16), with an extended period of perfect salt rejection. However, the permeate conductivity rapidly increased after 9 hours, indicating an occurrence of pore wetting. A further increase of ATRP reaction time for zwitterionic polymer grafting resulted in a significant improvement of MD performance; the JANUS QF-2h membrane exhibited not only a constant water flux but also a nearly perfect salt rejection throughout the MD fouling test (Figure 3.16).

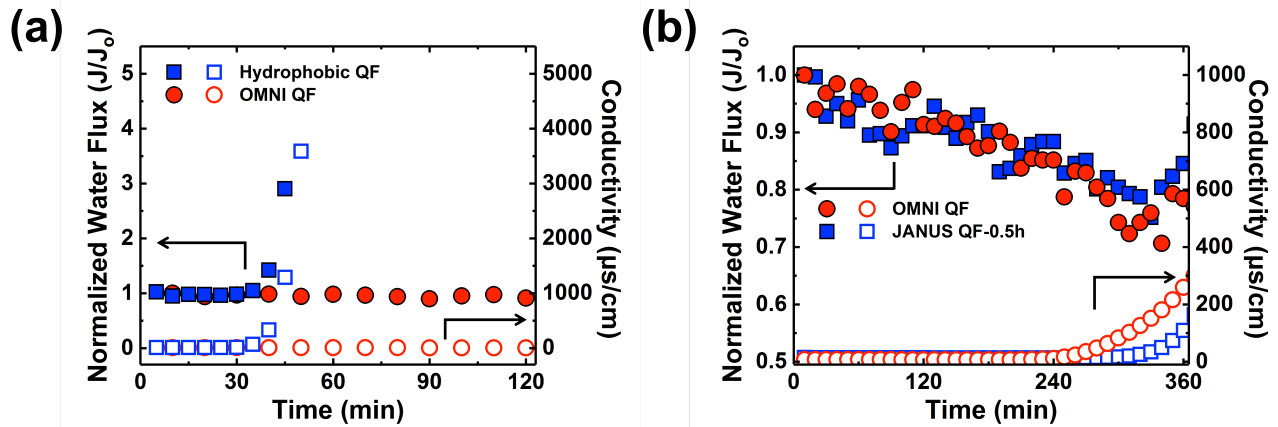


Figure 3.15 Comparison of wetting and fouling behaviors of the hydrophobic QF, OMNI QF, and JANUS QF-0.5h membranes in DCMD tests using a saline oil-in-water emulsion containing 1 M NaCl, 0.5 g L^{-1} crude oil, and 0.03 g L^{-1} TWEEN 20 at 60°C as the feed solution and deionized water at 20°C as the permeate solution. (a) Normalized water flux, J/J_0 , and permeate conductivity of the hydrophobic QF (square symbols) and OMNI QF (circle symbols) membranes, where the hydrophobic QF membrane exhibits poor wetting resistance. (b) Normalized water flux, J/J_0 , and permeate conductivity of the OMNI QF (circle symbols) and JANUS QF-0.5h (square symbols) membranes. The flux decline for both membranes with comparable rates indicates a similar fouling propensity. The rapid increase of conductivity after approximately 240 minutes indicates pore wetting. The initial water fluxes (J_0) of the hydrophobic QF, OMNI QF, and JANUS QF-0.5h membranes were 26.3 ± 0.4 , 15.8 ± 1.5 , and $18.4 \pm 0.8 \text{ L m}^{-2} \text{ h}^{-1}$, respectively.

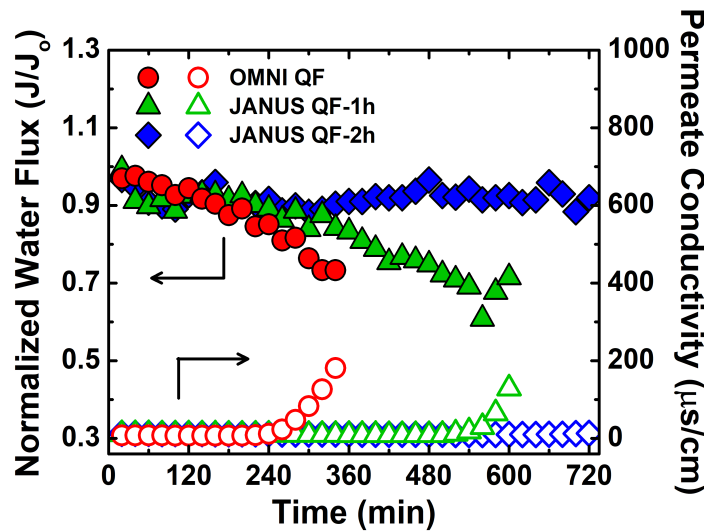


Figure 3.16 Time traces of normalized water flux, J/J_0 , and permeate conductivity of the OMNI QF (circle symbols), JANUS QF-1h (triangle symbols), and JANUS QF-2h (diamond symbols) membranes using a saline oil-in-water emulsion containing 1 M NaCl, 0.5 g L^{-1} crude oil, and 0.03 g L^{-1} TWEEN 20 at 60°C as the feed solution and deionized water at 20°C as the permeate solution. The initial water fluxes (J_0) of the OMNI QF, JANUS QF-1h, and JANUS QF-2h membranes were 15.8 ± 1.5 , 17.5 ± 1.5 , and $15.5 \pm 0.3 \text{ L m}^{-2} \text{ h}^{-1}$, respectively.

This observation presents the idea that the hydrophilic modification markedly enhances the fouling resistance, consistent with the static oil-fouling test (Figure 3.13), and does not exert detrimental effects on the wetting resistance. Still, mechanisms of the nonoccurrence of pore wetting in the JANUS QF-2h membrane as well as the observed oil-fouling-induced wetting in OMNI QF, JANUS QF-0.5h, and JANUS QF-1h membranes are rather speculative. Although omniphobic membranes are generally resistant to wetting by surfactant-containing, low-surface-tension feedwater,¹⁴⁻¹⁶ simultaneous fouling and wetting of omniphobic MD membranes treating foulant-containing feedwater have been reported.^{21,60} Consistent with previous fouling studies, membranes with an insufficient zwitterionic coating (i.e., OMNI QF, JANUS QF-0.5h, and JANUS QF-1h membranes) do not seem to effectively block hydrophobic-hydrophobic interaction between the oil droplets and the underlying omniphobic porous layer. Consequently, adsorption of the surfactant-bound oil droplets on the membrane pore surfaces still occurs, allowing the membrane pores to be covered by surfactants and subsequently leading to wetting.⁶¹ Meanwhile, the JANUS QF-2h membrane effectively prevents the adsorption of surfactant-bound oil droplets, deterring surfactant adsorption on the pore induced by oil fouling (as surfactant carriers). While free surfactant molecules (unbound to oil droplets) can readily pass through the hydrophilic layer and access the omniphobic inner layer of the JANUS QF-2h membrane, its high wetting resistance keeps the membrane unwetted. In addition, a recent study reported that the hydrophilic surface layer on MD membranes may reduce the access of surfactant molecules to the hydrophobic inner layer, partially contributing to wetting prevention.²² Taken together, our results suggest that a zwitterionic polymer layer of a sufficient quantity confers omniphobic membranes with an effective mechanism for both fouling and wetting prevention. This is also consistent with the previous study where a sufficient amount and thickness of the zwitterionic polymer layer is required to have an effective fouling resistance.⁴⁹

4. Conclusion

In this study, we fabricated Janus membranes by grafting a zwitterionic polymer brush layer through surface-initiated ATRP on an omniphobic membrane substrate for treating saline oily wastewaters through MD. The zwitterionic polymer layer was confined only on the membrane surface, and the surface hydrophilicity (on the polymer-grafted side) of the fabricated membrane can be tuned by controlling the polymerization duration. Even with the hydrophilic surface modification, the remaining part of the Janus membrane still maintained an excellent omniphobicity, resisting the wicking of both water and organic solvents (e.g., ethanol and hexane), and showed a stable desalination performance in MD tests with low-surface-tension ($\sim 33 \text{ mN m}^{-1}$) feedwater. We also performed oil-fouling MD experiments using a crude-oil-in-saline water (1 M NaCl) emulsion as a feedwater that mimics highly saline oily wastewaters. The omniphobic membrane without a hydrophilic layer was prone to severe oil fouling, and pore wetting eventually occurred. Janus membranes fabricated with a longer duration of the ATRP reaction exhibited a lower rate of water flux decline and more robust wetting resilience; Janus membranes modified with an ATRP reaction time of 2 hours exhibited a constant water flux and nearly complete salt rejection over the entire MD testing period. This superior MD performance of Janus membranes proves that an exceptionally hydrophilic zwitterionic polymer layer and a liquid-repelling omniphobic porous layer can be integrated without compromising each other's wetting property, through surface-initiated ATRP that allows for a robust chemical bonding between the two different layers and for a precise control of zwitterionic polymer layer thickness.

To the best of our knowledge, this study is the first to integrate a hydrophilic polymer layer on an omniphobic porous substrate with chemical bonding through a highly controllable ATRP reaction, which is expected to offer a more robust integration than those relying on physical integration. Our fabricated Janus membrane had showed excellent MD performance when treating synthetic wastewater. We anticipate that Janus membranes can significantly expand the applicability of MD for water reclamation from more challenging industrial highly saline wastewaters. Future research will need to be directed to (1) investigating the MD performance of the Janus membrane and (2) exploring the design and fabrication of a high-performance MD membrane for treating complex industrial wastewaters.

References

1. Li, C.; Li, X.; Du, X.; Tong, T.; Cath, T. Y.; Lee, J., Antiwetting and Antifouling Janus Membrane for Desalination of Saline Oily Wastewater by Membrane Distillation. *ACS Applied Materials & Interfaces* **2019**, *11*, 18456-18465.
2. Judd, S.; Jefferson, B., *Membranes for Industrial Wastewater Recovery and Re-Use*. Elsevier: Oxford, 2003.
3. WWAP (World Water Assessment Programme). *The United Nations World Water Development Report 4: Managing Water under Uncertainty and Risk*; UNESCO: Paris, 2012.
4. Fakhru'l-Razi, A.; Pendashteh, A.; Abdullah, L. C.; Biak, D. R. A.; Madaeni, S. S.; Abidin, Z. Z., Review of Technologies for Oil and Gas Produced Water Treatment. *Journal of Hazardous Materials* **2009**, *170*, 530-551.
5. Jiménez, S.; Micó, M. M.; Arnaldos, M.; Medina, F.; Contreras, S., State of the Art of Produced Water Treatment. *Chemosphere* **2018**, *192*, 186-208.
6. Greenlee, L. F.; Lawler, D. F.; Freeman, B. D.; Marrot, B.; Moulin, P., Reverse Osmosis Desalination: Water Sources, Technology, and Today's Challenges. *Water Research* **2009**, *43*, 2317-2348.
7. Coday, B. D.; Xu, P.; Beaudry, E. G.; Herron, J.; Lampi, K.; Hancock, N. T.; Cath, T. Y., The Sweet Spot of Forward Osmosis: Treatment of Produced Water, Drilling Wastewater, and Other Complex and Difficult Liquid Streams. *Desalination* **2014**, *333*, 23-35.
8. Riley, S. M.; Ahoor, D. C.; Oetjen, K.; Cath, T. Y., Closed Circuit Desalination of O&G Produced Water: An Evaluation of NF/RO Performance and Integrity. *Desalination* **2018**, *442*, 51-61.
9. Shaffer, D. L.; Arias Chavez, L. H.; Ben-Sasson, M.; Romero-Vargas Castrillón, S.; Yip, N. Y.; Elimelech, M., Desalination and Reuse of High-Salinity Shale Gas Produced Water: Drivers, Technologies, and Future Directions. *Environmental Science & Technology* **2013**, *47*, 9569-9583.
10. Alkhudhiri, A.; Darwish, N.; Hilal, N., Membrane Distillation: A Comprehensive Review. *Desalination* **2012**, *287*, 2-18.
11. Khayet, M., Membranes and Theoretical Modeling of Membrane Distillation: A Review. *Advances in Colloid and Interface Science* **2011**, *164*, 56-88.
12. Deshmukh, A.; Boo, C.; Karanikola, V.; Lin, S.; Straub, A. P.; Tong, T.; Warsinger, D. M.; Elimelech, M., Membrane Distillation at the Water-Energy Nexus: Limits, Opportunities, and Challenges. *Energy & Environmental Science* **2018**, *11*, 1177-1196.
13. Wang, P.; Chung, T.-S., Recent Advances in Membrane Distillation Processes: Membrane Development, Configuration Design and Application Exploring. *Journal of Membrane Science* **2015**, *474*, 39-56.
14. Boo, C.; Lee, J.; Elimelech, M., Engineering Surface Energy and Nanostructure of Microporous Films for Expanded Membrane Distillation Applications. *Environmental Science & Technology* **2016**, *50*, 8112-8119.
15. Lin, S.; Nejati, S.; Boo, C.; Hu, Y.; Osuji, C. O.; Elimelech, M., Omniphobic Membrane for Robust Membrane Distillation. *Environmental Science & Technology Letters* **2014**, *1*, 443-447.

16. Lee, J.; Boo, C.; Ryu, W.-H.; Taylor, A. D.; Elimelech, M., Development of Omniphobic Desalination Membranes Using a Charged Electrospun Nanofiber Scaffold. *ACS Applied Materials & Interfaces* **2016**, *8*, 11154-11161.
17. Oetjen, K.; Giddings, C. G. S.; McLaughlin, M.; Nell, M.; Blotevogel, J.; Helbling, D. E.; Mueller, D.; Higgins, C. P., Emerging Analytical Methods for the Characterization and Quantification of Organic Contaminants in Flowback and Produced Water. *Trends in Environmental Analytical Chemistry* **2017**, *15*, 12-23.
18. Pardue, M. J.; Castle, J. W.; Rodgers, J. H.; Huddleston, G. M., Treatment of Oil and Grease in Produced Water by a Pilot-Scale Constructed Wetland System Using Biogeochemical Processes. *Chemosphere* **2014**, *103*, 67-73.
19. Zuo, G.; Wang, R., Novel Membrane Surface Modification to Enhance Anti-Oil Fouling Property for Membrane Distillation Application. *Journal of Membrane Science* **2013**, *447*, 26-35.
20. Wang, Z.; Hou, D.; Lin, S., Composite Membrane with Underwater-Oleophobic Surface for Anti-Oil-Fouling Membrane Distillation. *Environmental Science & Technology* **2016**, *50*, 3866-3874.
21. Huang, Y.-X.; Wang, Z.; Jin, J.; Lin, S., Novel Janus Membrane for Membrane Distillation with Simultaneous Fouling and Wetting Resistance. *Environmental Science & Technology* **2017**, *51*, 13304-13310.
22. Chew, N. G. P.; Zhao, S.; Malde, C.; Wang, R., Polyvinylidene Fluoride Membrane Modification via Oxidant-Induced Dopamine Polymerization for Sustainable Direct-Contact Membrane Distillation. *Journal of Membrane Science* **2018**, *563*, 31-42.
23. Du, X.; Zhang, Z.; Carlson, K. H.; Lee, J.; Tong, T., Membrane Fouling and Reusability in Membrane Distillation of Shale Oil and Gas Produced Water: Effects of Membrane Surface Wettability. *Journal of Membrane Science* **2018**, *567*, 199-208.
24. Chew, N. G. P.; Zhao, S.; Malde, C.; Wang, R., Superoleophobic Surface Modification for Robust Membrane Distillation Performance. *Journal of Membrane Science* **2017**, *541*, 162-173.
25. Yang, H.-C.; Zhong, W.; Hou, J.; Chen, V.; Xu, Z.-K., Janus Hollow Fiber Membrane with a Mussel-Inspired Coating on the Lumen Surface for Direct Contact Membrane Distillation. *Journal of Membrane Science* **2017**, *523*, 1-7.
26. Wang, K.; Hou, D.; Wang, J.; Wang, Z.; Tian, B.; Liang, P., Hydrophilic Surface Coating on Hydrophobic PTFE Membrane for Robust Anti-Oil-Fouling Membrane Distillation. *Applied Surface Science* **2018**, *450*, 57-65.
27. Sun, W.; Shen, F.; Wang, Z.; Zhang, Y.; Wan, Y., An Ultrathin, Porous and In-Air Hydrophilic/Underwater Oleophobic Coating Simultaneously Increasing the Flux and Antifouling Property of Membrane for Membrane Distillation. *Desalination* **2018**, *445*, 40-50.
28. Lin, P.-J.; Yang, M.-C.; Li, Y.-L.; Chen, J.-H., Prevention of Surfactant Wetting with Agarose Hydrogel Layer for Direct Contact Membrane Distillation Used in Dyeing Wastewater Treatment. *Journal of Membrane Science* **2015**, *475*, 511-520.
29. Mohammadi Ghaleni, M.; Al Balushi, A.; Kaviani, S.; Tavakoli, E.; Bavarian, M.; Nejati, S., Fabrication of Janus Membranes for Desalination of Oil-Contaminated Saline Water. *ACS Applied Materials & Interfaces* **2018**, *10*, 44871-44879.
30. Sun, Q.; Su, Y.; Ma, X.; Wang, Y.; Jiang, Z., Improved Antifouling Property of Zwitterionic Ultrafiltration Membrane Composed of Acrylonitrile and Sulfobetaine Copolymer. *Journal of Membrane Science* **2006**, *285*, 299-305.
31. Zhao, J.; Shi, Q.; Luan, S.; Song, L.; Yang, H.; Shi, H.; Jin, J.; Li, X.; Yin, J.; Stagnaro, P., Improved Biocompatibility and Antifouling Property of Polypropylene Non-Woven Fabric

Membrane by Surface Grafting Zwitterionic Polymer. *Journal of Membrane Science* **2011**, *369*, 5-12.

32. Liu, C.; Lee, J.; Ma, J.; Elimelech, M., Antifouling Thin-Film Composite Membranes by Controlled Architecture of Zwitterionic Polymer Brush Layer. *Environmental Science & Technology* **2017**, *51*, 2161-2169.

33. Blackman, L. D.; Gunatillake, P. A.; Cass, P.; Locock, K. E. S., An Introduction to Zwitterionic Polymer Behavior and Applications in Solution and at Surfaces. *Chemical Society Reviews* **2019**, *48*, 757-770.

34. Chang, Y.; Liao, S.-C.; Higuchi, A.; Ruaan, R.-C.; Chu, C.-W.; Chen, W.-Y., A Highly Stable Nonbiofouling Surface with Well-Packed Grafted Zwitterionic Polysulfobetaine for Plasma Protein Repulsion. *Langmuir* **2008**, *24*, 5453-5458.

35. Xing, C.-M.; Meng, F.-N.; Quan, M.; Ding, K.; Dang, Y.; Gong, Y.-K., Quantitative Fabrication, Performance Optimization and Comparison of PEG and Zwitterionic Polymer Antifouling Coatings. *Acta Biomaterialia* **2017**, *59*, 129-138.

36. Choi, H.; Jung, Y.; Han, S.; Tak, T.; Kwon, Y.-N., Surface Modification of SWRO Membranes Using Hydroxyl Poly(Oxyethylene) Methacrylate and Zwitterionic Carboxylated Polyethyleneimine. *Journal of Membrane Science* **2015**, *486*, 97-105.

37. Palacio, L.; Prádanos, P.; Calvo, J. I.; Hernández, A., Porosity Measurements by a Gas Penetration Method and Other Techniques Applied to Membrane Characterization. *Thin Solid Films* **1999**, *348*, 22-29.

38. Stöber, W.; Fink, A.; Bohn, E., Controlled Growth of Monodisperse Silica Spheres in the Micron Size Range. *J. Colloid Interface Sci.* **1968**, *26*, 62-69.

39. Smith, E. A.; Chen, W., How to Prevent the Loss of Surface Functionality Derived from Aminosilanes. *Langmuir* **2008**, *24*, 12405-12409.

40. Liao, Y.; Wang, R.; Tian, M.; Qiu, C.; Fane, A. G., Fabrication of Polyvinylidene Fluoride (PVDF) Nanofiber Membranes by Electro-Spinning for Direct Contact Membrane Distillation. *J. Memb. Sci.* **2013**, *425-426*, 30-39.

41. Ye, G.; Lee, J.; Perreault, F.; Elimelech, M., Controlled Architecture of Dual-Functional Block Copolymer Brushes on Thin-Film Composite Membranes for Integrated "Defending" and "Attacking" Strategies against Biofouling. *ACS Appl. Mater. Interfaces*. **2015**, *7*, 23069-23079.

42. Liu, C.; Lee, J.; Small, C.; Ma, J.; Elimelech, M., Comparison of Organic Fouling Resistance of Thin-Film Composite Membranes Modified by Hydrophilic Silica Nanoparticles and Zwitterionic Polymer Brushes. *J. Memb. Sci.* **2017**, *544*, 135-142.

43. Hester, J. F.; Banerjee, P.; Won, Y. Y.; Akthakul, A.; Acar, M. H.; Mayes, A. M., ATRP of Amphiphilic Graft Copolymers Based on PVDF and Their Use as Membrane Additives. *Macromolecules* **2002**, *35*, 7652-7661.

44. Chen, Y.; Liu, D.; Deng, Q.; He, X.; Wang, X., Atom Transfer Radical Polymerization Directly from Poly(Vinylidene Fluoride): Surface and Antifouling Properties. *Journal of Polymer Science Part A: Polymer Chemistry* **2006**, *44*, 3434-3443.

45. He, F.; Luo, B.; Yuan, S.; Liang, B.; Choong, C.; Pehkonen, S. O., PVDF Film Tethered with RGD-Click-Poly(Glycidyl Methacrylate) Brushes by Combination of Direct Surface-Initiated ATRP and Click Chemistry for Improved Cytocompatibility. *RSC Advances* **2014**, *4*, 105-117.

46. Han, Y.; Song, S.; Lu, Y.; Zhu, D., A Method to Modify PVDF Microfiltration Membrane via ATRP with Low-Temperature Plasma Pretreatment. *Applied Surface Science* **2016**, *379*, 474-479.

47. Yeow, J.; Chapman, R.; Gormley, A. J.; Boyer, C., Up in the Air: Oxygen Tolerance in Controlled/Living Radical Polymerisation. *Chemical Society Reviews* **2018**, *47*, 4357-4387.
48. Li, M.; Katsouras, I.; Piliego, C.; Glasser, G.; Lieberwirth, I.; Blom, P. W. M.; de Leeuw, D. M., Controlling the Microstructure of Poly(Vinylidene-Fluoride) (PVDF) Thin Films for Microelectronics. *J. Mater. Chem. C* **2013**, *1*, 7695-7702.
49. Davenport, D. M.; Lee, J.; Elimelech, M., Efficacy of Antifouling Modification of Ultrafiltration Membranes by Grafting Zwitterionic Polymer Brushes. *Sep. Purif. Technol.* **2017**, *189*, 389-398.
50. Matijević, E.; Pethica, B. A., The Properties of Ionized Monolayers. Part 1.—Sodium Dodecyl Sulphate at the Air/Water Interface. *Trans. Faraday Soc.* **1958**, *54*, 1382-1389.
51. Tuteja, A.; Choi, W.; Ma, M.; Mabry, J. M.; Mazzella, S. A.; Rutledge, G. C.; McKinley, G. H.; Cohen, R. E., Designing Superoleophobic Surfaces. *Science* **2007**, *318*, 1618-1622.
52. Kota, A. K.; Kwon, G.; Tuteja, A., The Design and Applications of Superomniphobic Surfaces. *NPG Asia Materials* **2014**, *6*, e109.
53. Zorn, G.; Baio, J. E.; Weidner, T.; Migonney, V.; Castner, D. G., Characterization of Poly(Sodium Styrene Sulfonate) Thin Films Grafted from Functionalized Titanium Surfaces. *Langmuir* **2011**, *27*, 13104-13112.
54. Socrates, G., *Infrared and Raman Characteristic Group Frequencies: Tables and Charts*. 3rd ed.; John Wiley & Sons Ltd.: West Sussex, UK, 2004.
55. Matyjaszewski, K.; Miller, P. J.; Shukla, N.; Immaraporn, B.; Gelman, A.; Luokala, B. B.; Siclován, T. M.; Kickelbick, G.; Vallant, T.; Hoffmann, H.; Pakula, T., Polymers at Interfaces: Using Atom Transfer Radical Polymerization in the Controlled Growth of Homopolymers and Block Copolymers from Silicon Surfaces in the Absence of Untethered Sacrificial Initiator. *Macromolecules* **1999**, *32*, 8716-8724.
56. Matyjaszewski, K., Atom Transfer Radical Polymerization (ATRP): Current Status and Future Perspectives. *Macromolecules* **2012**, *45*, 4015-4039.
57. Poll, H. U.; Schladitz, U.; Schreiter, S., Penetration of Plasma Effects into Textile Structures. *Surface and Coatings Technology* **2001**, *142-144*, 489-493.
58. Angulakshmi, N.; Nahm, K. S.; Choi, J.-M.; Hwang, Y. J.; Stephan, A. M., Electrochemical Properties of Coconut Shell Flour-Incorporated Poly(Vinylidenehexafluoropropylene)-Based Electrospun Membranes for Lithium Batteries. *Science of Advanced Materials* **2013**, *5*, 606-611.
59. Brzoska, J. B.; Azouz, I. B.; Rondelez, F., Silanization of Solid Substrates: A Step toward Reproducibility. *Langmuir* **1994**, *10*, 4367-4373.
60. Boo, C.; Lee, J.; Elimelech, M., Omniphobic Polyvinylidene Fluoride (PVDF) Membrane for Desalination of Shale Gas Produced Water by Membrane Distillation. *Environmental Science & Technology* **2016**, *50*, 12275-12282.
61. Wang, Z.; Lin, S., Membrane Fouling and Wetting in Membrane Distillation and Their Mitigation by Novel Membranes with Special Wettability. *Water Research* **2017**, *112*, 38-47.